and M and Γ are the mass and width of the resonance.[11]

We have used this model to fit the $\pi^- p$ data from this experiment along with 50 data from Ref. 2 at 2.08, 2.18, and 2.28 GeV/c, nine data from Ref. 5 at 180° and nine data from Ref. 7. The χ^2 for the fit to 138 data points is 510. In fitting these data, we have restricted the parametrization originally proposed by Crittenden *et al.*[9] To reduce the number of adjustable parameters we required that a be the same for all trajectories, as mentioned above.[12] We have also found it possible to use $b=0.5$ for seven of the 13 trajectories. (This value of b gives a fairly good fit to the elasticities of the Δ_δ recurrences.) For the other six trajectories, b was varied[13] between the empirically chosen limits $0.2 \leq b \leq 10$. As shown in Table II, Γ_1 and x_1 were adjusted for several of the lowest-lying resonances in order to improve the agreement of the model with the data. We make no claims of uniqueness for the model we have employed or the parameter values we have used. The chief value of this calculation is that we show that it is possible to reproduce the rich structure observed in $\pi^- p$ backward elastic angular distributions using only direct-channel resonances. We are presently applying this model to all existing $\pi^\pm p \to p\pi^\pm$ and $\pi^- p$ charge-exchange data between 2 and 5 GeV/c for $90° \leq \theta_{\text{c.m.}} \leq 180°$.[14]

The observed structure in $\pi^- p \to p\pi^-$ angular distributions in Fig. 1 is not obtained by Regge-pole calculations using the exchange of a single (Δ_δ) trajectory.[15]

We are grateful for the help we have received during this experiment from the staffs of the Argonne ZGS and the I. U. Research Computing Center. We thank Dennis Duncan and Craig McPherson for their patient assistance in preparing the film for measurement and in running our automatic scanner. We appreciate the contributions of J. P. Chandler, Hugh Martin, Don Meyer, H. W. Paik, K. Potocki, and W. F. Prickett to initial stages of this experiment. Professor Marc Ross, Professor Enrico Predazzi, and Professor Don Lichtenberg have been particularly helpful with the theoretical interpretation of the data.

[11] Reference 9 uses a truncated resonant amplitude to fit the $\pi^+ p \to p\pi^+$ data from Ref. 1.

[12] For a discussion of the width function $\Gamma(s)$ see A. Degasperis and E. Predazzi, Nuovo Cimento (to be published).

[13] The fitting routine used was STEPIT, a Fortran IV subroutine copyright 1965 by J. P. Chandler, which is available from the Indiana University Research Computing Center.

[14] M. Ciftan and G. Patsakos have recently compared forward pion-nucleon scattering data with results of four interference models which can be constructed from Regge, resonance, and absorptive amplitudes. They find that a Regge-resonance model based, in part, on Ref. 9 gives a good fit to the data up to $s \cong 25$ GeV^2. M. Ciftan and G. Patsakos, Phys. Rev. D **1**, 2156 (1970).

[15] E. Paschos, Phys. Rev. Letters **21**, 1855 (1968).

PHYSICAL REVIEW D VOLUME 1, NUMBER 11 1 JUNE 1970

Study of $\pi^+ p$ Four-Prong Interactions from 2.95 to 4.08 GeV/c*

DAVID BROWN,† GEORGE GIDAL,‡ AND ROBERT W. BIRGE
Lawrence Radiation Laboratory, University of California, Berkeley, California 94720

AND

SUN-YIU FUNG, WARREN JACKSON,§ AND ROBERT T. POE
Physics Department, University of California, Riverside, California 92502

(Received 13 January 1970)

In a study of the production mechanism of quasi-two-body final states at the five incident π^+ momenta 2.95, 3.2, 3.5, 3.75, and 4.08 GeV/c, approximately 40 000 events with four outgoing charged particles were investigated. The cross sections for the processes $\pi^+ p \to N^{*++}\rho$, $\pi^+ p \to N^{*++}\omega$, $\pi^+ p \to N^{*++}\eta$, and $\pi^+ p \to N^{*++} f$ have been measured as a function of the pion energy. The differential cross sections and the decay density-matrix elements are discussed in terms of one-meson-exchange models [with absorption (OPEA) and with form factor (OPEW)] and Regge models. For the $N^{*++}\rho$ and the $N^{*++}\omega$ reactions, the joint-decay matrix elements are calculated. The formation of $N^*(2850)$ in the direct channel is also investigated.

INTRODUCTION

IN an effort to extend the available data on production mechanisms of multipion final states, we have studied four-prong events of the types

$$\pi^+ p \to \pi^+ p \pi^+ \pi^- \quad (1)$$

$$\to \pi^+ p \pi^+ \pi^- \pi^0 \quad (2)$$

$$\to \pi^+ \pi^+ \pi^+ n \pi^-, \quad (3)$$

* Work performed under the auspices of the U. S. Atomic Energy Commission.

† Present address: United States Public Health Service, Bureau of Radiological Health, Rockville, Md.

‡ Current address: Physics Department, Tel Aviv University, Ramat Aviv, Israel.

§ Present address: Physics Department, University of Toronto, Toronto, Canada.

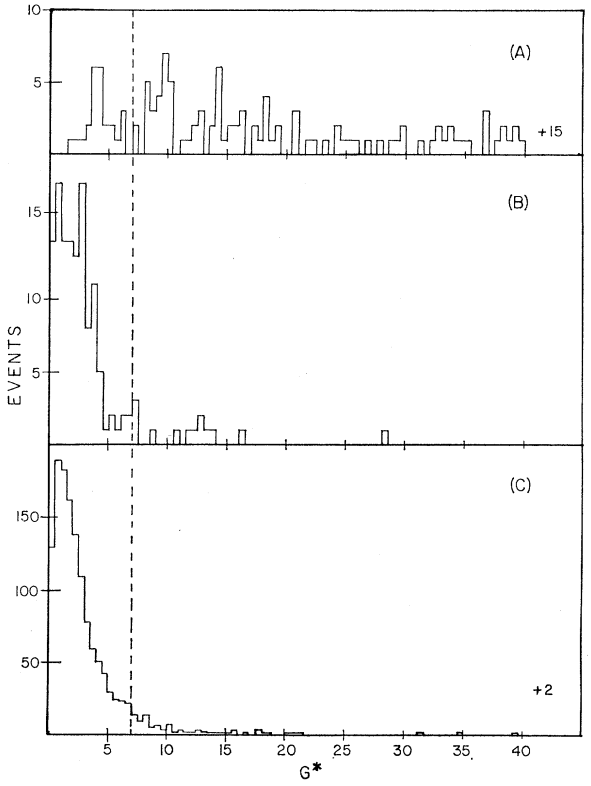

FIG. 1. G^* distributions for the ambiguous 4C-fit events for the permutation with (A) the highest and (B) the lowest G^*, and (C) for the unambiguous 4C fits.

at the five incident π^+ momenta 2.95, 3.2, 3,5, 3.75, and 4.08 GeV/c.[1–12] These reactions have long been known to be dominated by such quasi-two-body final states as $N^{*++}\rho^0$, $N^{*++}\omega^0$, pA_2, etc., produced predominantly with small momentum transfer to the baryon, and the cross sections and angular distributions of these processes are studied. The $I=\frac{3}{2}$ $N^*(2850)$ lies within this energy region, and an attempt was made to determine the magnitude of its contribution to the cross section. Preliminary results appeared in a previous article,[13] and further details are available in another work,[14] which will be referred to as A.

I. EXPERIMENTAL PROCEDURE

The 72-in. hydrogen bubble chamber was exposed to a separated π^+ beam to obtain 0.29 μb/event of pion path length. The film was scanned for four-prong interactions, and these events were measured on the flying-spot-digitizer (FSD) automatic measuring machine. The FOG-CLOUDY-FAIR system of computer programs was used to reconstruct the events and to constrain the events to those reactions of intereest. Over 90% of the measured events survived processing.

A major problem in this experiment is the proton contamination in the beam which varied from 3 to 10%

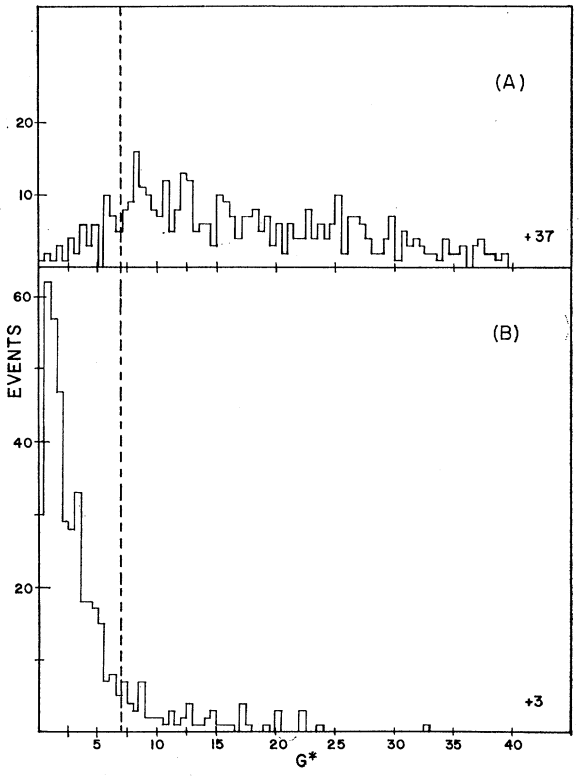

FIG. 2. G^* distributions for the events constraining to a permutation of both reactions (1) and (2) for (A) the best (lowest G^*) reaction-(2) permutation which constrained and (B) the best reaction-(1) permutation.

[1] H. Foelsche and H. Kraybill, Phys. Rev. **134**, B1138 (1964).
[2] J. K. Kopp, A. Shapiro, and A. Erwin, Phys. Rev. **123**, 301 (1961).
[3] P. Daronian, A. Daudin, M. Jabiol, C. Lewin, C. Kochowski, B. Ghidini, S. Mongelli, and V. Picciarelli, Nuovo Cimento **41A**, 503 (1966).
[4] J. A. Johnson and H. L. Kraybill, Bull. Am. Phys. Soc. **9**, 70 (1964).
[5] F. E. James and H. L. Kraybill, Phys. Rev. **142**, 896 (1966).
[6] N. Gelfand (Ph.D. thesis), Report No. CU-1932-239 Nevis-137, 1965 (unpublished).
[7] N. Armenise, B. Ghidini, V. Picciarelli, A. Romano, G. Kayas, J. Laberrigue-Frolow, J. Tridon, L. Vigneron, and T. P. Yiou, Nuovo Cimento **41A**, 159 (1966).
[8] S. Yamamoto, J. Smith, D. Rahm, and J. Lloyd, Phys. Rev. **140**, B730 (1965).
[9] M. Abolins, R. Lander, W. Mehlhop, N. Xuong, and P. Yager, Phys. Rev. **11**, 381 (1963).
[10] B. Shen, (Ph.D. thesis), UCRL Report No. UCRL-16170, 1965 (unpublished).
[11] Aachen-Berlin-Birmingham-Bonn-Hamburg-London (I.C.)-München Collaboration, Phys. Rev. **138**, B897 (1965).
[12] M. Deutschmann, R. Schulte, H. Weber, W. Woischnig, C. Grote, J. Klugow, S. Nowak, S. Brandt, V. Cocconi, O. Czyzewski, P. Dalpiaz, G. Kellner, and D. Morrison, Phys. Letters **12**, 356 (1964).
[13] D. Brown, G. Gidal, R. W. Birge, R. Bacastow, S. Fung, W. Jackson, and R. Pu, Phys. Rev. Letters **19**, 664 (1967).
[14] D. Brown, UCRL Report No. UCRL-18254, 1968 (unpublished).

for most of the film but was 24% for the 4.08-GeV/c exposure. In order to get a better quantitative understanding of this contamination, the measured four-prong events were constrained to the following reactions

$$p p \rightarrow p p \pi^+ \pi^- \quad (4)$$

$$\rightarrow p p \pi^+ \pi^- \pi^0 \quad (5)$$

$$\rightarrow p \pi^+ \pi^+ \pi^- n. \quad (6)$$

The ratio of the number of events constraining to these reactions to those constraining to the corresponding pion beam hypotheses (N_p/N_π), when compared to the ratio of the respective cross sections, was used to determine the fraction of protons in the pion-plus-proton beam. Also, using the number of events constraining to both pion and proton hypotheses and the ratio N_p/N_π, an estimate of the maximum proton-event contamination of the final-event sample may be obtained. The contaminations at the various momenta are (0.03±0.008), (0.10±0.01), (0.19±0.02), (0.45±0.04), and (2.6±0.1)%, respectively.

Because of the beam contamination, it was desirable to obtain the total pion path length by some method independent of measurement of this contamination. This could be accomplished by normalizing to the cross-section for δ rays with momenta greater than 18 MeV/c (i.e., sufficiently large that the δ-ray cross section for production by a beam proton is negligible). A scan for strong interactions on beam tracks with these δ rays was made over about 20% of the film with the δ-ray momentum being measured. From the known cross section for these δ rays, the total $\pi^+ + \mu^+$ track length could be obtained; and from the number of strong interactions occurring on these tracks and the total $\pi^+ p$ interaction cross section, the muon contamination could be estimated. Because of the paucity of data, this latter was done for the entire experiment, rather than for each momentum separately, with an assumed $1/p$ (lifetime effect) dependence upon incident momentum, and was found to be (5±2)%. The δ-ray normalization yielded values of (1.21±0.05), (2.33±0.08), (2.20±0.09), (1.80±0.06), (2.10±0.06)×10^7 cm pion path length at the five energies, respectively. As a check, a scan for all strong interactions was made on a sample of the film and used in conjunction with the proton contamination data to normalize to the $\pi^+ p$ total cross section. This method gave quite satisfactory agreement with the δ-ray results.

Extensive use was made of the automatic ionization measurements available from the FSD,[15] and the events were required to satisfy ionization criteria in addition to the usual kinematic, fiducial, and momentum requirements, which are described in detail in A.

[15] H. White, S. Buckman, D. Hall, E. Hurwitz, L. Meissner, J. Smith, and F. Stannard, UCRL Report No. URCL-9457, 1960 (unpublished). A more comprehensive reference is A. Rosenfeld and W. Humphrey, Ann. Rev. Nucl. Sci. **13**, 103 (1963).

TABLE I. Normalization and cross sections for reactions (1)–(3) (4C, π^0, n).

Momentum (GeV/c)	Reaction	Normalization (10^{-3} mb/event)	Good events	σ (mb)
2.95	4C	3.67±0.28	798	2.93±0.25
	π^0	3.50±0.35	850	2.98±0.31
	n	3.37±0.34	157	0.53±0.07
			1805	6.44±0.61
3.19	4C	1.73±0.12	1683	2.91±0.21
	π^0	1.54±0.14	2195	3.38±0.31
	n	1.40±0.13	421	0.59±0.06
			4299	6.88±0.56
3.53	4C	1.71±0.11	1943	3.33±0.24
	π^0	1.60±0.15	2280	3.64±0.34
	n	1.44±0.13	433	0.63±0.06
			4656	7.60±0.63
3.74	4C	2.26±0.15	1498	3.39±0.24
	π^0	2.06±0.18	1851	3.79±0.35
	n	1.88±0.17	488	0.84±0.09
			3797	8.03±0.66
4.08	4C	2.05±0.14	1383	2.83±0.21
	π^0	1.78±0.16	2125	3.78±0.36
	n	1.57±0.15	613	0.97±0.10
			4121	7.58±0.65
		(10^{-4} mb/event)		
Combined	4C	4.22±0.13	7305	3.09±0.10
	π^0	3.84±0.16	9301	3.57±0.15
	n	3.48±0.15	2072	0.72±0.03
			18678	7.37±0.26

The ionization information was furnished by the FSD as the fraction (H_m) of the scans of a given track for which a bubble was encountered.[16] A similar number (H_c) was computed from the particle's known momentum and assumed mass, and was normalized using the minimally ionizing beam tracks. Corrections were made for the orientation of the track relative to the plane of the camera, and of the projection of the track relative to the scan direction. It was found that the measured ionization was also dependent upon position in the chamber, so corrections were made for this effect as well. The quantity G^* was then defined to be the average, for all of the tracks for which ionization information was received, of the quantity $(H_c - H_m)^2/D_h^2$, where D_h was the estimated error on the ionization measurement. It was used to resolve ambiguities and filter out incorrect mass assignments. The number of ambiguities would have been doubled without its use.

Figure 1 shows the G^* distributions for one experiment (3.53 GeV/c) for events of reaction (1) which were (a) ambiguous (more than one mass assignment kinematically allowed), with the largest G^* histogrammed, (b) ambiguous with the smallest G^*, and (c)

[16] G. Borreani, and D. Hall, UCRL Physics Note PB-119, 1967 (unpublished).

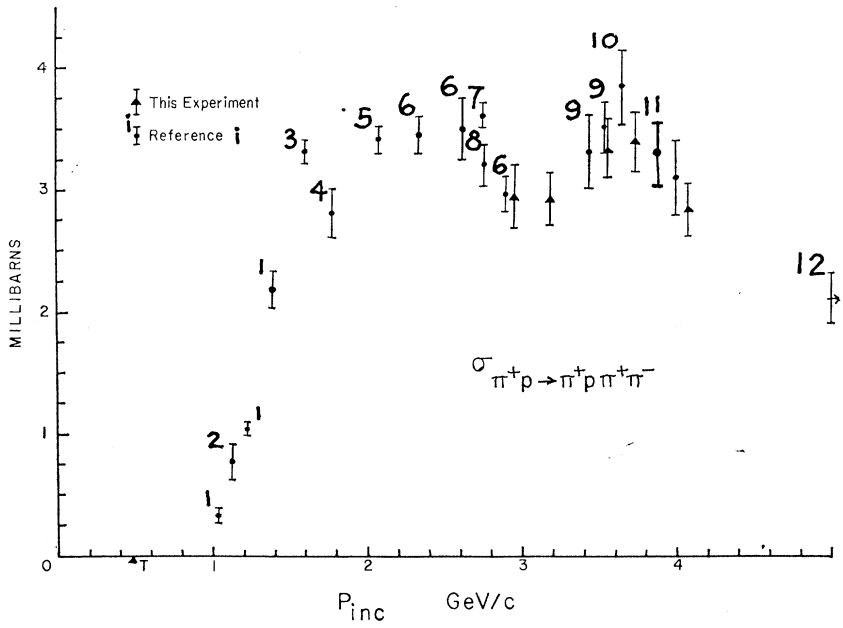

FIG. 3. Cross section for $\pi^+p \to \pi^+p\pi^-\pi^+$.

unambiguous. This shows the extent to which G^* could be used to differentiate between the different hypotheses. Further, Fig. 2 shows the G^* distributions for the reactions (1) and (2) overlap events for (a) the best (by G^*) reaction-(2) hypothesis which fit and (b) for the reaction-(1) hypothesis fitting. Only those cases (96%) for which different tracks were fitted as the proton under the two hypotheses were used. Clearly G^* offers a good method for choosing the correct hypothesis, and also, as expected, 4C fits [four-constraint fits—reaction (1)] are more reliable than 1C fits [reactions (2) and (3)].

Some of the events are still constrained to more than one hypothesis. These ambiguous events, amounting to 11% of the good-event sample, were examined on the scan table. Roughly 30% of these could not be resolved by ionization or secondary interaction information and were assigned on the basis of the lower kinematic χ^2 value, with the greater reliability of 4C than 1C fits being taken into consideration.

The final values for the mb/event ratios are given in Table I, along with the resulting cross sections for reactions (1)–(3).

II. $N^*(2850)$

The cross sections for reactions (1)–(3) are shown in Figs. 3 and 4.[17] Values from other experiments are included in order to give a better understanding of the energy dependence of the cross sections. Those found in this experiment are seen to agree fairly well with earlier work, at least to within the rather substantial errors involved.

[17] A complete set of invariant-mass and momentum-transfer distributions for each of these reactions is to be found in A.

In particular, previous results indicated the possibility of a broad enhancement in the cross section for reaction (1) in the region of the $N^*(2850)$. This was supported both by the general trend of the experimental cross sections and by structure in the $M(\pi^+p\pi^+\pi^-)$ invariant-mass distribution of 8-GeV/c π^+p six-prong events (Bardadin-Otwinowska *et al.*[18]). Quite striking confirmation of this has been obtained, although the evidence is not completely conclusive because of the large experimental errors. Despite the evident arbitrariness of any attempt to put a smooth curve through the experimental points and the difficulty in drawing a suitable background, this had been done and is shown in Fig. 5. The resulting very crude estimate of the cross section for formation of $N^*(2850)$ with subsequent decay into $\pi^+p\pi^+\pi^-$ is exhibited in the inset to that figure. The resonance mass and width are seen to be roughly 2800 and 200 MeV, respectively, which are not unreasonably far from the total cross section values of 2850 and 400 MeV. The height, however, is suprisingly large. It has been estimated as about 0.65 mb, which is 84% of the (0.77±0.06)-mb figure of Citron *et al.*[19] for the $N^*(2850)$ contribution to the total cross section.

In Sec. III it will be seen that the relative fraction of $N^{*++}\rho$ is nearly constant with energy for this experiment. Thus, the structure of the $N^{*++}\rho$ cross section is just that of the cross section for reaction (1). With the same reservations expressed above, this leads to a peak value of 0.25±0.10 mb for the decay of the $N^{*++}(2850)$ into $N^{*++}\rho$.

[18] M. Bardadin-Otwinowska, M. Danysz, T. Hofmokl, S. Otwinoski, H. Piotrowska, R. Sosnowski, M. Szeptycka, and A. Wroblewski, Phys. Letters **21**, 357 (1966).

[19] A. Citron, W. Galbraith, T. Kycia, B. Leontic, R. Phillips, A. Rousset, and P. Sharp, Phys. Rev. **144**, 1101 (1966).

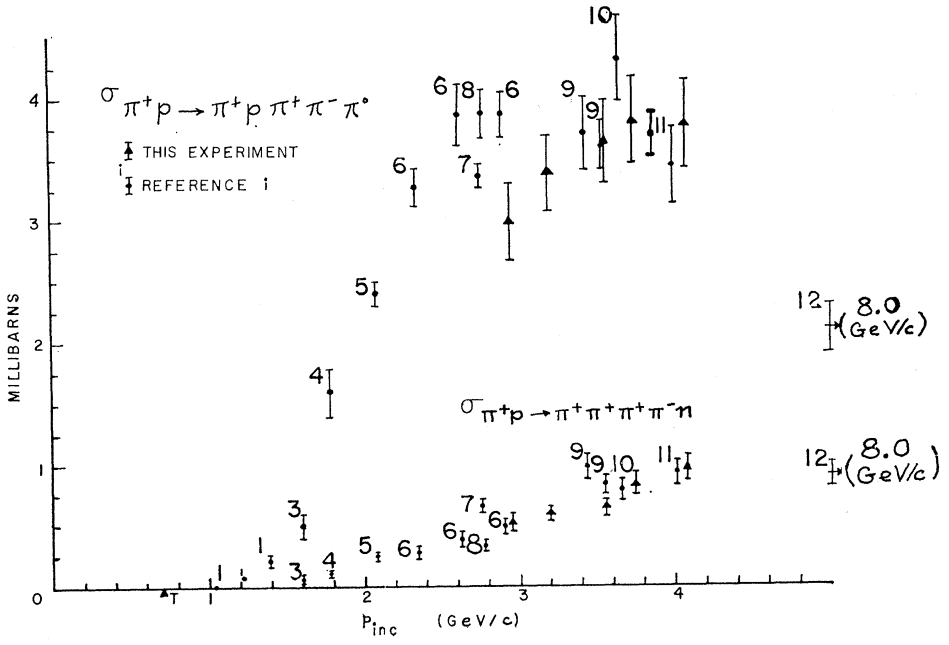

FIG. 4. Cross sections for $\pi^+p \to \pi^+p\pi^+\pi^-\pi^0$ and $\pi^+p \to \pi^+\pi^+\pi^+\pi^-n$.

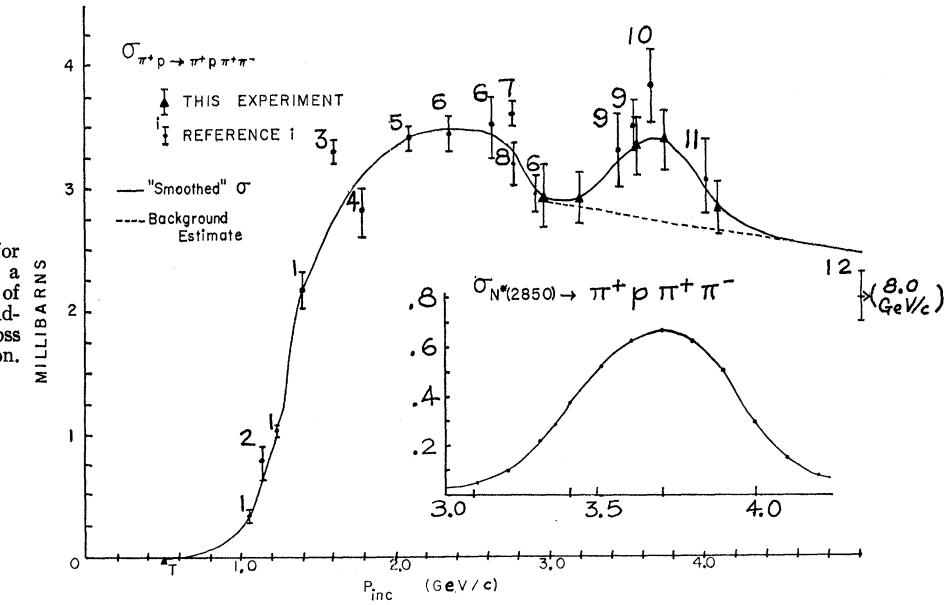

FIG. 5. Cross section for $\pi^+p \to \pi^+p\pi^+\pi^-$, with a smooth-line interpolation of the experimental points yielding an estimate of the cross section for $N^*(2850)$ formation.

III. DOUBLE-RESONANCE PRODUCTION

As noted in Sec. II, reactions (1) and (2) are dominated by double-resonance channels, in particular by $N^{*++}\rho^0$ and $N^{*++}\omega^0$ production, respectively. The additional final states of $N^{*++}f^0$ and $N^{*++}\eta^0$ will also be considered in this section, although they are produced less copiously.

The analysis of these reactions divides naturally into three levels of sophistication. Treated as strictly two-body channels, the relevant variables are the masses of the two systems, the momentum transfer from the incident to the outgoing $B=0$ (or, equivalently, $B=1$) "particle," and the total c.m. energy. Production cross sections for the various two-body final states are presented. Next, recognizing that the final-state particles are unstable, the decay angular distributions (density-matrix elements) in the appropriate rest frames are of interest. Finally, the possibility of correlations between the two decays is considered and the joint-density matrix elements examined.

Comparisons are made with the one-meson-exchange model with absorption (OMEA) of Jackson[20] and a

[20] J. D. Jackson, Nuovo Cimento 34, 1644 (1964); J. T. Donohue, Ph.D. thesis, Univeristy of Illinois, 1967 (unpublished).

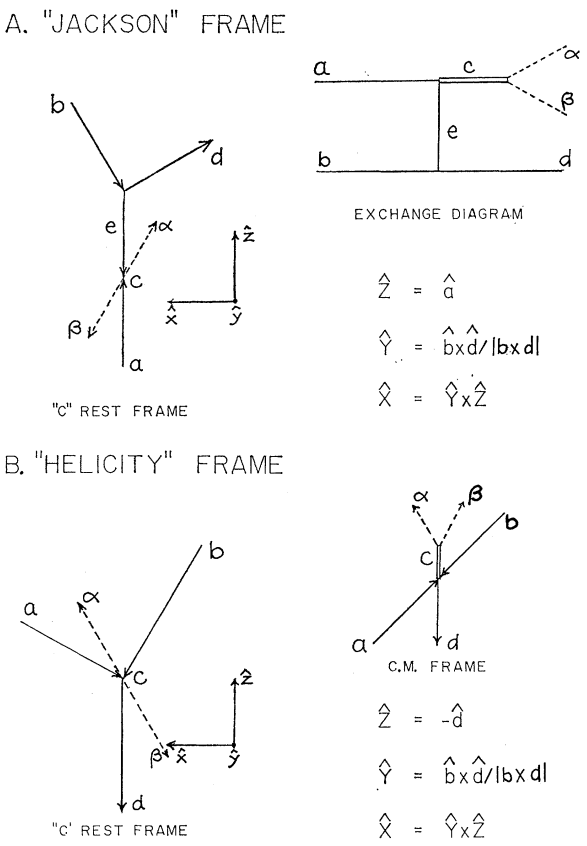

FIG. 6. Reference frames used in the description of resonance decay angular distributions.

form-factor approach suggested by Wolf (OMEW).[21] The OMEA is especially useful because it may be used to predict the density-matrix elements as well as the momentum-transfer distributions. Following a suggestion of Jackson, it has been altered slightly to take into account the effects of the finite widths of the resonances concerned. Background effects are discussed.

Discussion of several points in the Regge-pole model will be make, although no detailed fits have been attempted.

It should be noted that the reference frame used here in the description of the decay distributions is not that commonly employed (Jackson frame). It is customary to take the z axis along the direction of the respective incident particle in the decay particle's rest frame. However, the helicity states (which constitute the basis used for the density-matrix elements) are most easily described using axes with z along the direction of the transformation from the c.m. to the decay c.m. frame. The transformation which customarily is then used to rotate the density matrix into the Jackson frame is dependent upon the values of the masses of the final-state particles, and is hence the source of some inconvenience and confusion when the finite widths of the resonances are taken into account. For ease in comparing the density matrices of this with other experiments, the experimental values are given for both systems. The reference frames are illustrated in Fig. 6.

One complicating aspect of these double-resonance channels is the presence of the two positive pions, with one being assigned to each of the two final-state systems. This is a complication in two respects: (1) It introduces an ambiguity when both combinations lie within the chosen mass bands—e.g., $M(\pi_1^+p)$ and $M(\pi_2^+p)$ both lie between 1.12 and 1.32 GeV and $M(\pi_2^+\pi^-)$ and $M(\pi_1^+\pi^-)$ both lie between 0.68 and 0.86 GeV. (2) It increases the difficulty of estimating background when the reflection as well as the tails of the process enhance the neighboring region of the triangle plot. Fortunately, the peripheral nature of these reactions enables one to differentiate between the positive pions in a reasonable manner. In this analysis the "correct" combination for the small percentage of ambiguous events has been chosen on the basis of the smaller momentum transfer.

Evidence that this is a reasonable procedure is presented in Figs. 7 and 8, where the invariant masses of the $\pi^+\pi^-$, π^+p, and $\pi^+\pi^-\pi^0$, π^+p combinations are shown. Choosing the combination with the smaller momentum transfer is seen to enhance the N^*,ρ and N^*,ω signals. Fewer than 2% of the events in each sample are so affected.

A. $\pi^+p \rightarrow N^{*++}\rho^0$

$N^*\rho^0$ production accounts for roughly 40% of reaction (1). The $N^*\rho$ cross sections were estimated from fits to the triangle plots of Fig. 9, with an attempt being made to represent the background with something slightly more realistic than pure phase space. A Monte Carlo program [Appendix C in A] was used to generate events according to six possible final states:

$$\pi^+p \rightarrow \pi^+p\pi^+\pi^- \text{ (phase space)} \quad (7)$$

$$\rightarrow N^{*++}\rho^0 \ (e^{8t}) \quad (8)$$

$$\rightarrow N^{*++}f^0 \ (e^{7t}) \quad (9)$$

$$\rightarrow pA_1 \ (e^{10t}) \quad (10)$$

$$\searrow \pi^+\rho^0$$

TABLE II. Logarithmic slope of the momentum transfer and t' distributions for the intervals (a) $0.2<-t<0.5$ $(\text{GeV}/c)^2$, (b) $0<t'<0.2$ $(\text{GeV}/c)^2$.

P_{inc} (GeV/c)	(a) $A_{N^*\rho}$ $(\text{GeV}/c)^{-2}$	(b) $A'_{N^*\rho}$ $(\text{GeV}/c)^{-2}$
2.95	6.1±1.3	12.7±0.7
3.19	6.9±0.9	12.2±0.9
3.53	8.3±0.8	11.6±0.8
3.74	7.1±1.2	11.3±0.8
4.08	7.8±1.0	12.6±1.1
All	7.3±0.5	11.8±0.4

[21] G. Wolf, Phys. Rev. Letters 19, 925 (1967).

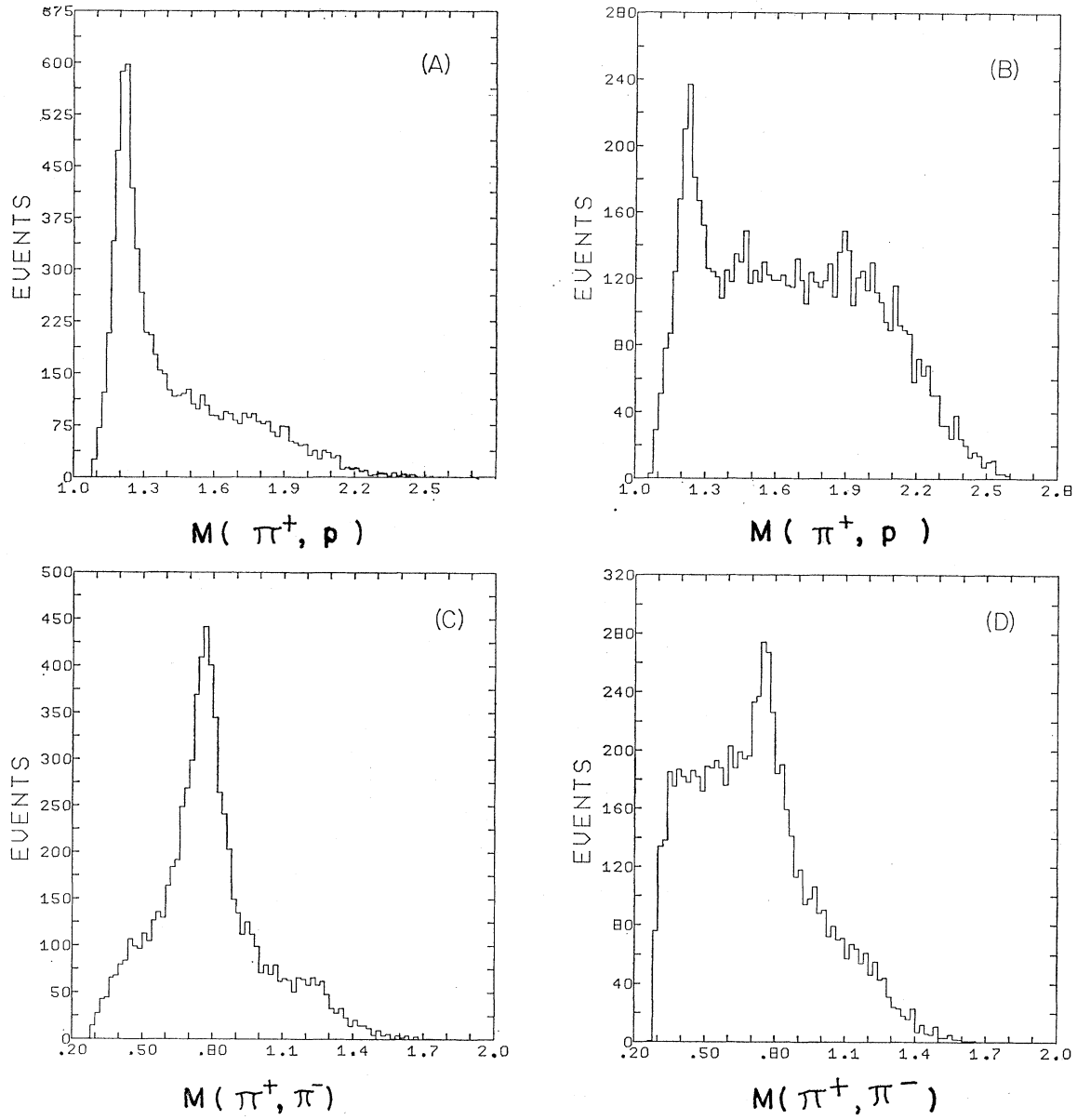

FIG. 7. π^+p (top) and $\pi^+\pi^-$ (bottom) invariant-mass distributions for those combinations with the lesser (left) and greater (right) momentum transfer from the proton to the π^+p system.

$$\pi^+p \longrightarrow pA_2 \qquad (e^{6t}) \tag{11}$$
$$\searrow$$
$$\pi^+\rho^0$$
$$\longrightarrow \pi^+N^{*++}(1700)\ (e^{6t}). \tag{12}$$
$$\searrow$$
$$\pi^-N^{*++}$$

The resonance parameters used are based on those in the January 1968 Particle Data Tables[22] and are listed in (A). The events were generated having the exponential momentum-transfer dependence shown in parentheses (in the momentum-transfer variable appropriate for each reaction) and then weighted according to resonance Breit-Wigners. The $\pi^+\pi^-$–π^+p scatter plots of these events were used in fitting the corresponding data distribution at each energy. The following limitations should be noted: (1) Only the $\pi^+\pi^-$–π^+p distribution was fitted, so that the resonance parameters and relative fractions of the latter three reactions are not to be taken seriously. Details concerning these "background" reactions are only included here, phenomeno-

[22] A. H. Rosenfeld *et al.*, Rev. Mod. Phys. **40**, 77 (1968); A. Barbaro-Galtieri, S. E. Derenzo, L. R. Price, A. Rittenberg, A. H. Rosenfeld, N. Barash-Schmidt, C. Bricman, M. Roos, P. Söding, and C. G. Wohl, *ibid.* **42**, 87 (1970).

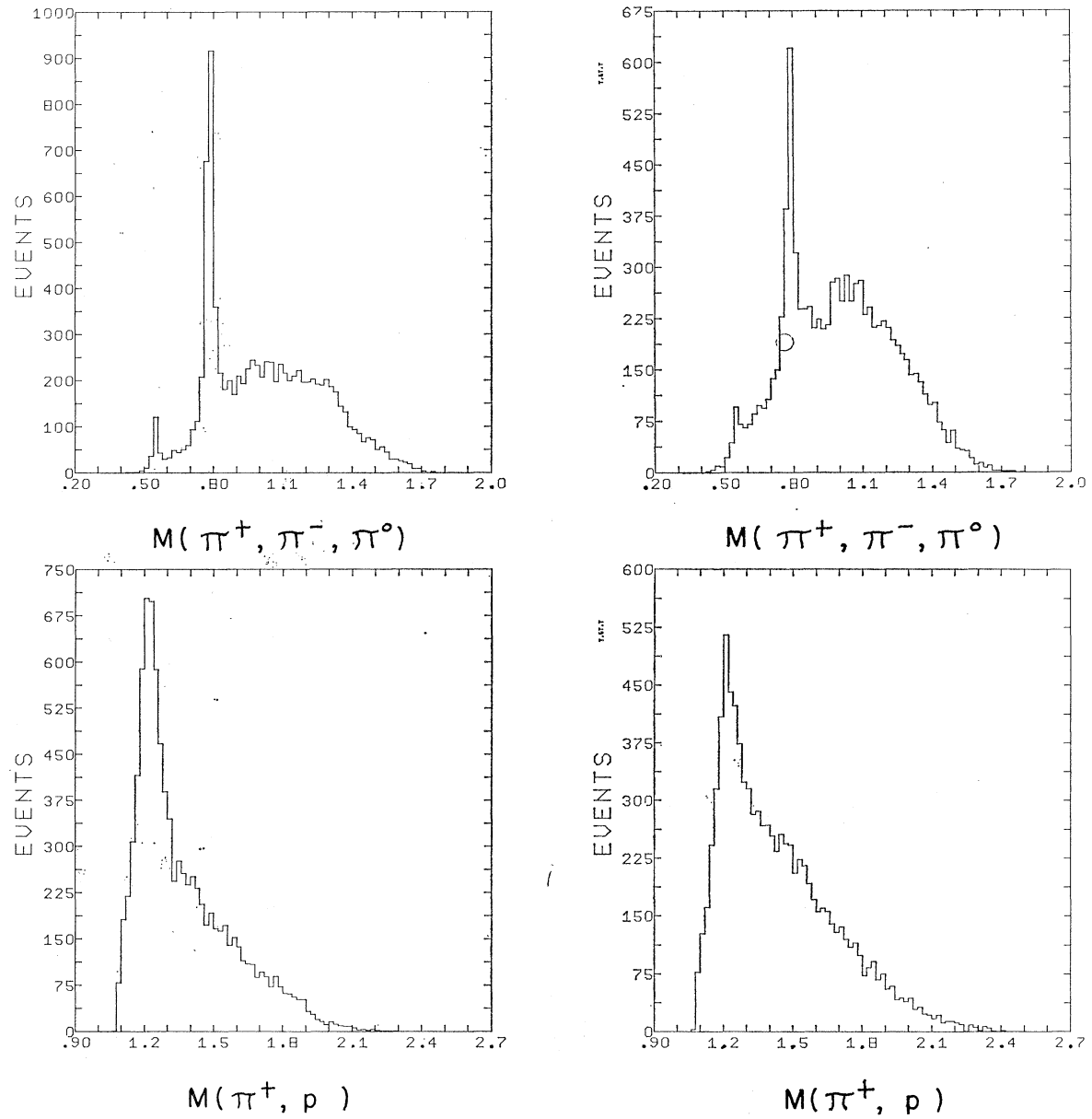

FIG. 8. $\pi^+\pi^-\pi^0$ (top) and π^+p (bottom) invariant-mass distributions for those combinations with the lesser (left) and greater (right) momentum transfer from the proton to the π^+p system.

logically, in order to parametrize the background better. (2) The weighting of the (100 000) Monte Carlo events of the respective reactions resulted in the effective number of events in each fitting distribution being comparable to the number in the data distribution, so that the theoretical errors are important in lowering the χ^2's. Therefore, the only parameters in which one may hold a reasonable degree of confidence are the fractions of $N^{*++}\rho^0$ and $N^{*++}f^0$ production. The corresponding cross sections in mb are plotted in Fig. 10.

Since the relative fraction of $N^{*++}\rho$ is found to be nearly constant with energy, the structure of the $N^{*++}\rho$ cross section is just that of the total 4C cross section. The N^*f cross section exhibits the expected near-threshold behavior, not being produced copiously until low momentum-transfer values are kinematically allowed.

For a more detailed analysis of the $N^{*++}\rho$ final state it was necessary to choose selection criteria such that an enriched sample of $N^{*++}\rho$ events would be obtained. Those events were taken with $M(\pi_i^+p)$ lying between 1.12 and 1.32 GeV and $M(\pi_j^+\pi^-)$ between 0.68 and 0.86 GeV. Ambiguities were resolved on the basis of momentum transfer—i.e., if $M(\pi_j^+p)$ and $M(\pi_i^+\pi^-)$

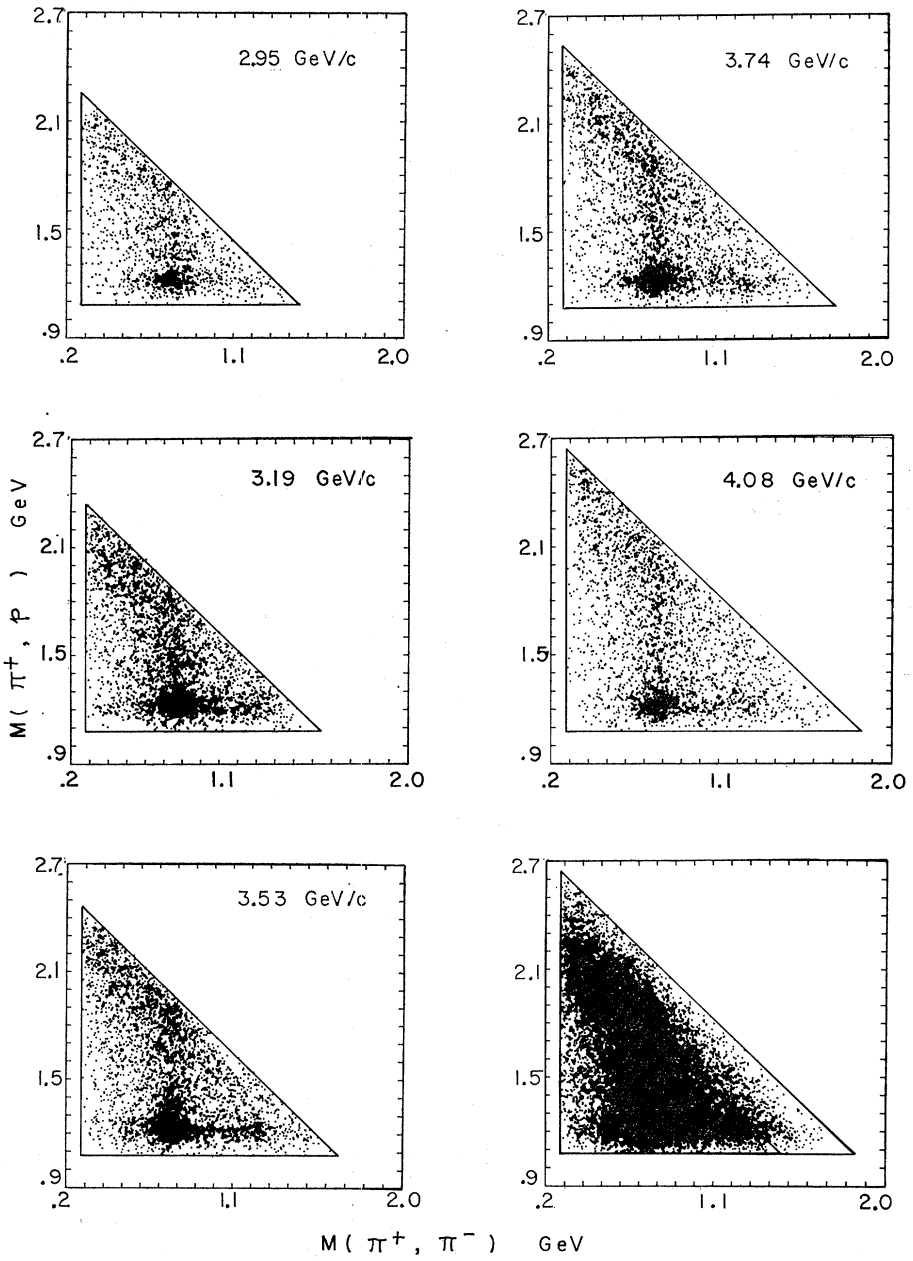

FIG. 9. $\pi^+p\to\pi^+\pi^-$ triangle plots for reactions (1) for the individual momenta and their sum. Both combinations are plotted for each event.

also lay within the requisite mass limits, the combination with the smaller momentum transfer from the proton to the "N^*" was chosen.

The distribution in production angle is shown in Fig. 11. The extent of the forward peaking is manifest, with over 60% of the events lying within the 5% of the $\cos\theta$ range which is greater than 0.9. Two other aspects of the data are noteworthy, however: (1) The "equatorial" region of $\cos\theta$ is increasingly depleted as the energy increases. (2) There is a small backward peak at the highest momenta. Part of (1) is of course accounted for by the approximate e^{At} behavior of the forward peak which, for constant A, requires shrinkage in the $\cos\theta$ peak with increasing energy. The effect persists, however, beyond the peak region.

In terms of the momentum transfer (Fig. 12), the most prominent feature of the forward peak is its nearly constant slope on a logarithmic scale. Column (a) of Table II gives the results of the fits to this slope. The interval $0.2<-t<0.5$ $(\mathrm{GeV}/c)^2$ has been used, since the boundary region extends to 0.2 $(\mathrm{GeV}/c)^2$ (at the lowest momentum), and a marked change in the slope occurs at about 0.5 $(\mathrm{GeV}/c)^2$. The average value of the slope is found to be about 7.3 ± 0.5 $(\mathrm{GeV}/c)^{-2}$.

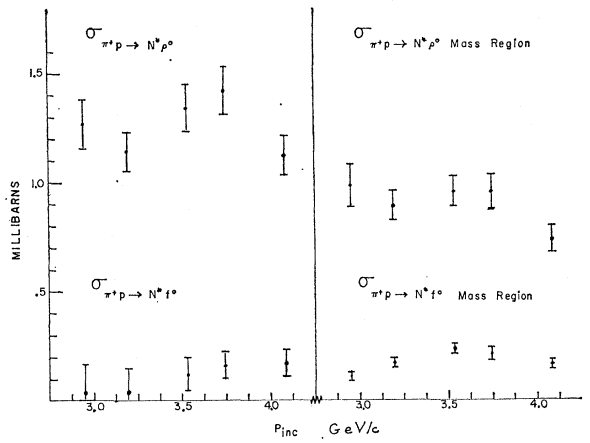

FIG. 10. Cross sections for $N^*\rho$ and N^*f production from the fit to the triangle plot and for production of events within $0.68 < M(\pi_i^+\pi^-) < 0.86$ GeV/c^2 for ρ, $1.17 < M(\pi_i^+\pi^-) < 1.31$ GeV/c^2 for f, and $1.12 < M(\pi_j^+ p) < 1.32$ GeV/c^2 for N^*.

Although a simple exponential fits the data quite well between 0.2 and 0.5 $(\text{GeV}/c)^2$, outside this range of $-t$ there are important discrepancies. In the vicinity of $-t = 0.5$ $(\text{GeV}/c)^2$ there is a radical change in slope [from $A = 7.3$ to $A \simeq 2$ $(\text{GeV}/c)^{-2}$] and perhaps even a "dip." The curve superimposed on the $-t$ distribution of Fig. 12 is that given by an exponential distribution with $A = 7.3$ $(\text{GeV}/c)^{-2}$, integrated over the $N^*\rho$ mass region (weighted by resonance Breit-Wigners) and summed over incident momenta [weighted as the number of events for $0.2 < -t < 0.5$ $(\text{GeV}/c)^2$]. It illustrates the success of the exponential fit above the boundary region and its complete failure within that region. In the region where the operation of the kinematic limits would be supposed to reduce the cross section, the experimental points in fact lie well above the extrapolation of a straight $e^{7.3t}$ dependence. For the region $0 < -t < 0.5$ $(\text{GeV}/c)^2$ the experimental distribution contains 68% more events than predicted by the exponential fit. Of course, theoretically this is not unexpected. Both OPEA and OPEW models predict distributions which are more-than-exponentially peaked in $-t$. The data amply confirm this.

There is some slight evidence for shrinkage in the data—i.e., for A being an increasing function of incident momentum, as the fitted value increases from 6.1 to 7.8 $(\text{GeV}/c)^{-2}$ in the interval studied. The evidence is hardly conclusive, however, since the highest value

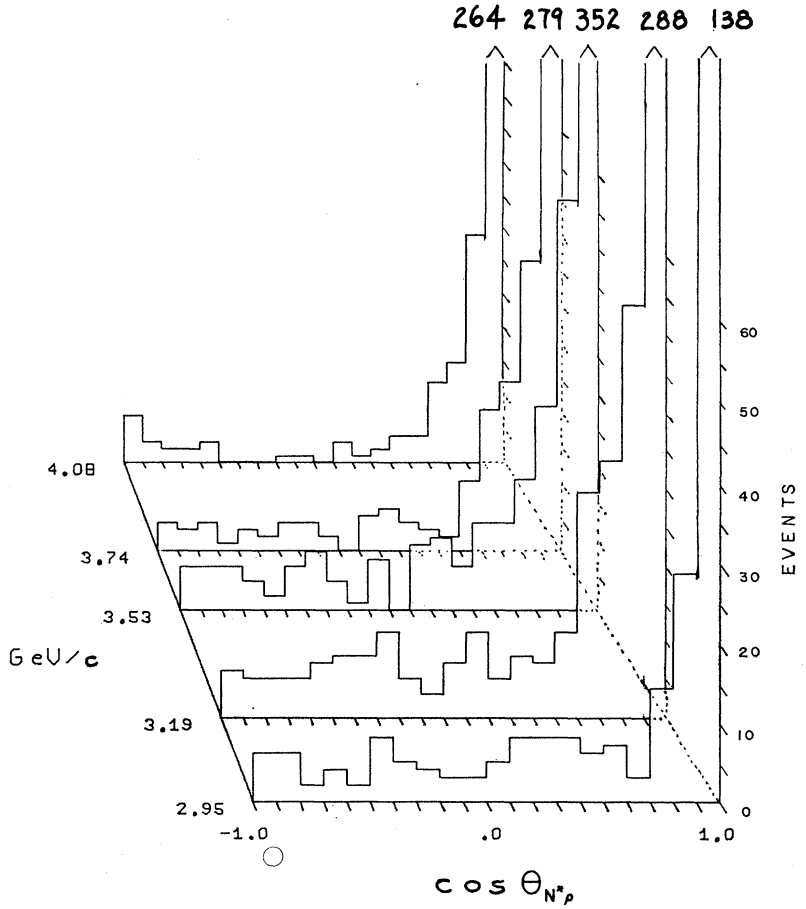

FIG. 11. $N^*\rho$-production cosine distributions at the five momenta. The forward peak is truncated and the number of events in it indicated above.

occurred at the central momentum and all of the values lie within errors of the average value.[23] Further, the values obtained for the central region of the $N^*\rho$ [$1.17<M(\pi^+p)<1.27$ GeV, $0.725<M(\pi^+\pi^-)<0.815$ GeV] do not domonstrate such a trend, although this is not surprising in view of the large errors accompanying them. The values for A are of course substantially lower than those obtained at higher energies, so that our data in combination with other results do demonstrate a quite strong increase of A with energy.[13]

As seen above, momentum transfer is an inconvenient variable to use when wide resonances are studied, because many of the events occur in the "boundary" region where interpretation of the data is difficult. In order to obviate this difficulty, it is useful to use the variable $t'=|t-t_{\min}|$, where $t_{\min}$ is calculated for each event and is the minimum value $-t$ could assume, given the masses of the two final-state systems for that event. Figure 13 gives experimental t' distributions together with the results of an exponential fit to the data. An exponential in t' was also fit to each momentum separately, and the results are shown in column (b) of Table II. The fits are quite good all the way from $t'=0$

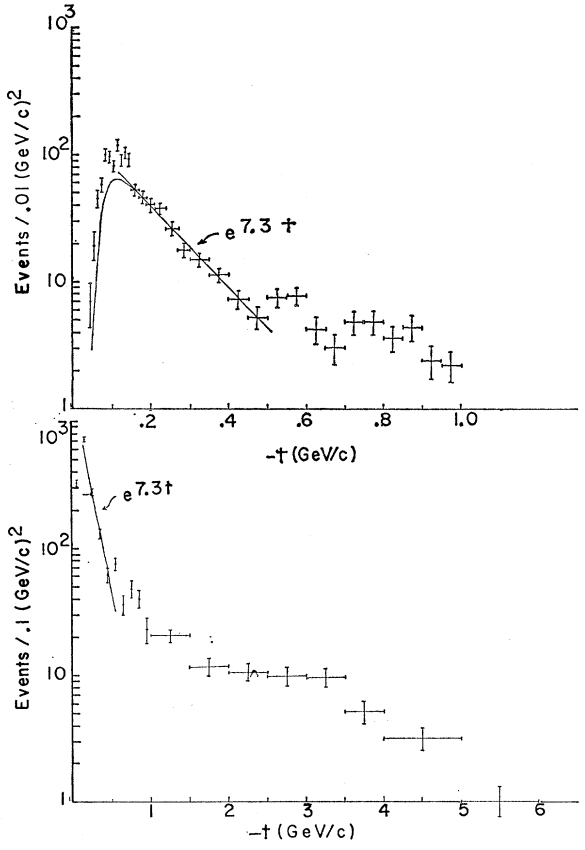

FIG. 12. $N^*\rho$ momentum-transfer distribution displayed over its entire range (bottom) and in fine detail (top).

[23] L. D. Jacobs [(Ph.D. thesis), UCRL Report No. UCRL-16877, 1966 (unpublished)] indicates that A may be expected to increase in the region of an s-channel resonance.

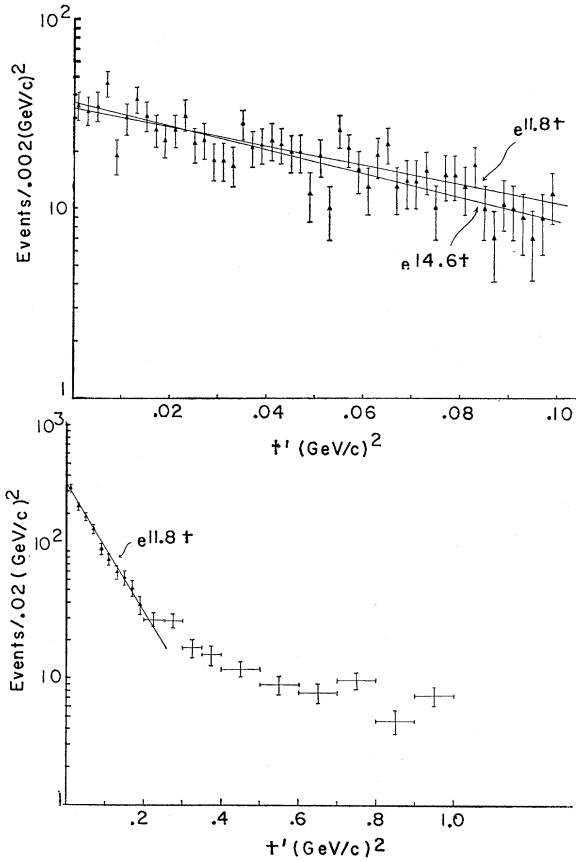

FIG. 13. $N^*\rho$ t' distribution displayed for $0<t'<0.1$ (GeV/c)^2 (top) and for $0<t'<1.0$ (GeV/c)^2 (bottom).

to 0.2 (GeV/c)^2 and vary little from energy to energy. In the very forward direction, from $t'=0$ to 0.05 (GeV/c)^2, the fitted value for A was 14.6 ± 2.0 (GeV/c)$^{-2}$, which is substantially greater than that obtained for the larger range of t' [11.8 ± 0.4 (GeV/c)$^{-2}$].

LeBellac has pointed out that if the pion Regge trajectory has a conspirator, i.e., another trajectory which crosses it at $t=0$, then the differential cross section for $\pi^+p\rightarrow N^{*++}\rho^0$ should have a dip in the forward direction. Neither the t nor t' distributions lend credibility to such predictions of a "turnover" in $d\sigma/dt$ at small t, although the $t_{\min}$ at our energies are rather large to explore this question. A similar experiment at 8 GeV/c incident momentum has more clearly demonstrated this effect. However, it should be pointed out that some of the background processes might be responsible for the peaking in the far forward direction. This possibility is currently being investigated.

In order to compare the momentum-transfer distribution of Fig. 12 with OPEA and OPEW predictions, the experimental distribution must be suitably normalized. Both the background events within the mass cuts and the $N^*\rho$ tail outside must be taken into account before applying the mb/event ratios of Table I. The back-

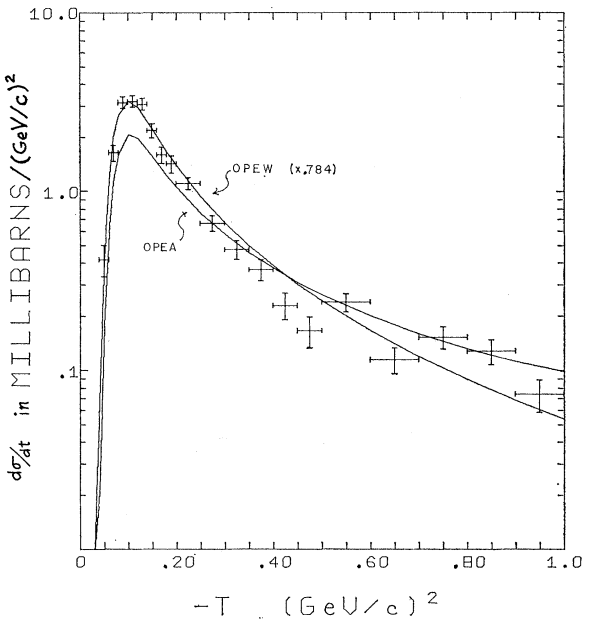

FIG. 14. $d\sigma/dt$ and $N^*\rho$ production in the $N^*\rho$ mass region showing OPEA and OPEW predictions as well as the experimental points.

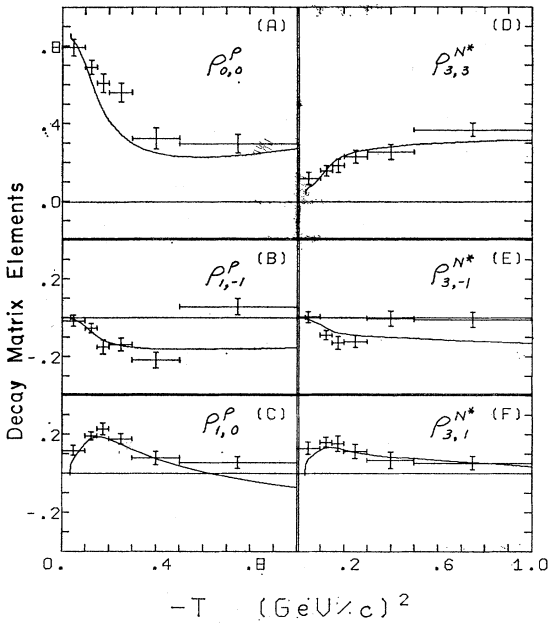

FIG. 15. $N^*\rho$-decay matrix elements as a function of momentum transfer, with the OPEA predictions being indicated by the solid line, for (A) $\rho_{0,0}{}^{\rho}$, (B) $\rho_{1,-1}{}^{\rho}$, (C) $\rho_{1,0}{}^{\rho}$, (D) $\rho_{3,3}{}^{N^*}$, (E) $\rho_{3,-1}{}^{N^*}$, (F) $\rho_{3,1}{}^{N^*}$.

ground was estimated with the aid of the Monte Carlo events previously used in fitting the $\pi^+p\to\pi^+\pi^-$ triangle plot.[14] A factor for the "tail" contribution was not used in normalizing $d\sigma/dt$: As with the theoretical curves, $d\sigma/dt$ is given for $N^*\rho$ production within the stated mass limits.

In Fig. 14, OPEA and OPEW curves are shown with the experimental distribution. The curves are the weighted averages of curves for the five incident momenta [weighted so the area under each curve, for the region $0<-t<0.5$ (GeV/c)^2, was equal to the number of events in that region at the corresponding momentum]. Also, the OPEW curve is multiplied by 0.784 (the background correction factor), since it seems to fit the data much better without a correction for background and since the OPEW parameters were obtained without background subtraction. Only the form-factor approach seems to yield a sufficiently steep slope for $d\sigma/dt$, although the OPEA gives a fair approximation to experiment. Note that the OPEA predictions are decreased by a factor of 3 by integrating over the $N^*\rho$ masses instead of assuming them to be stable (zero-width) particles.

For the analysis of the decay distribution we use the formalism given by Donohue[20] and parametrize the $N^*\rho$ joint distribution as follows:

$$
\begin{aligned}
W(\theta_c,\varphi_c,\theta_d,\varphi_d)=(1/16\pi^2)\{&1+\tfrac{1}{2}(1-3\rho_{00}{}^c)(1-3\cos^2\theta_c)-\tfrac{1}{2}(1-4\rho_{33}{}^d)(1-3\cos^2\theta_d)+R_8(1-3\cos^2\theta_c)(1-3\cos^2\theta_d)\\
&-3(\rho_{1,-1}{}^c\sin^2\theta_c\cos2\varphi_c+\sqrt{2}\rho_{10}{}^c\sin2\theta_c\cos\varphi_c)-2\sqrt{3}(\rho_{3,-1}{}^d\sin^2\theta_d\cos2\varphi_d+\rho_{3,1}{}^d\sin2\theta_d\cos\varphi_d)\\
&-3(1-3\cos^2\theta_d)[R_9\sin^2\theta_c\cos2\varphi_c+(1/\sqrt{2})R_{10}\sin2\theta_c\cos\varphi_c]-\sqrt{3}(1-3\cos^2\theta_c)\\
&\times(R_{11}\sin^2\theta_d\cos2\varphi_d+R_{12}\sin2\theta_d\cos\varphi_d)+3\sqrt{3}(\sin^2\theta_c\sin^2\theta_d)[R_{13}\cos(2\varphi_c+2\varphi_d)+R_{14}\cos(2\varphi_c-2\varphi_d)]\\
&+\sin^2\theta_c\sin2\theta_d[R_{15}\cos(2\varphi_c+\varphi_d)+R_{16}\cos(2\varphi_c-\varphi_d)]+(1/\sqrt{2})\sin2\theta_c\sin^2\theta_d\\
&\times[R_{17}\cos(\varphi_c+2\varphi_d)+R_{18}\cos(\varphi_c-2\varphi_d)]+(1/\sqrt{2})\sin2\theta_c\sin2\theta_d\\
&\times[R_{19}\cos(\varphi_c+\varphi_d)+R_{20}\cos(\varphi_c-\varphi_d)]\},
\end{aligned}
$$

where

(a) θ_c,φ_c, θ_d, and φ_d are the decay angles in either the helicity or Jackson frames for the ρ^0 and N^{*++}, respectively ($c\equiv\rho$, $d\equiv N^{*++}$);

(b) $\rho_{ij}{}^{\alpha}$ is the real part of the ijth density-matrix element for the αth particle;

(c) the R are combinations of joint-density-matrix elements given in Table III. The above distribution is given in terms of orthogonal but not orthonormal functions and the terms in $\rho_{ij}{}^{\alpha}$ constitute the decay distribution of the αth particle. The $\rho_{ij}{}^{\alpha}$ and R_k have been experimentally determined, by the method of moments, and are displayed in the figures which follow.

TABLE III. Relations between the angular-distribution parameters and the helicity-matrix elements, and their expression in terms of the decay angles. Only the real part of the helicity-matrix elements contributes; so, for convenience, $R_{\lambda_c\lambda_c';\lambda_d\lambda_d'}$ has been written for $\mathrm{Re}[R_{\lambda_c\lambda_c';\lambda_d\lambda_d'}]$. (As used below, $k=25\sqrt{3}/16$.)

Parameter	Helicity-matrix elements	Angular functions
$\rho_{0,0}{}^c$		$\frac{1}{2}\langle 5\cos^2\theta_c-1\rangle$
$\rho_{1,-1}{}^c$	$\rho_{mm'}{}^c=\sum_n R_{mm';nn}$	$-(5/4)\langle \sin^2\theta_c\cos 2\varphi_c\rangle$
$\rho_{1,1}{}^c$		$-(5/4\sqrt{2})\langle \sin 2\theta_c\cos\varphi_c\rangle$
$\rho_{3,3}{}^d$		$(1/8)\langle 7-15\cos^2\theta_d\rangle$
$\rho_{3,-1}{}^d$	$\rho_{nn'}{}^d=\sum_m R_{mm;nn'}$	$-(5\sqrt{3}/8)\langle \sin^2\theta_d\cos 2\varphi_d\rangle$
$\rho_{3,1}{}^d$		$-(5\sqrt{3}/8)\langle \sin 2\theta_d\cos\varphi_d\rangle$
R_8	$\frac{1}{2}(R_{11;33}+R_{11;-3,-3}-R_{11;-1,-1}-2R_{00,33}+2R_{00;11}-R_{11;11})$	$(25/16)\langle(1-3\cos^2\theta_c)(1-3\cos^2\theta_d)\rangle$
R_9	$R_{1,-1;33}-R_{1,-1;11}$	$-(25/16)\langle(1-3\cos^2\theta_d)\sin^2\theta_c\cos 2\varphi_c\rangle$
R_{10}	$R_{10;33}+R_{10;-3,-3}-R_{10;11}-R_{10;-1,-1}$	$-(25/8\sqrt{2})\langle(1-3\cos^2\theta_d)\sin 2\theta_c\cos\varphi_c\rangle$
R_{11}	$R_{11;3,-1}+R_{11;1,-3}-2R_{00;3,-1}$	$-k\langle(1-3\cos^2\theta_c)\sin^2\theta_d\cos 2\varphi_d\rangle$
R_{12}	$R_{11;31}+R_{11;-1,-3}-2R_{00;31}$	$-k\langle(1-3\cos^2\theta_c)\sin 2\theta_d\cos\varphi_d\rangle$
R_{13}	$R_{1,-1;3,-1}$	$k\langle\sin^2\theta_c\sin^2\theta_d\cos(2\varphi_c+2\varphi_d)\rangle$
R_{14}	$R_{1,-1;-13}$	$k\langle\sin^2\theta_c\sin^2\theta_d\cos(2\varphi_c-2\varphi_d)\rangle$
R_{15}	$R_{1,-1;31}$	$k\langle\sin^2\theta_c\sin 2\theta_d\cos(2\varphi_c+\varphi_d)\rangle$
R_{16}	$R_{1,-1;13}$	$k\langle\sin^2\theta_c\sin 2\theta_d\cos(2\varphi_c-\varphi_d)\rangle$
R_{17}	$R_{10;3,-1}+R_{10;1,-3}$	$k\sqrt{2}\langle\sin 2\theta_c\sin^2\theta_d\cos(\varphi_c+2\varphi_d)\rangle$
R_{18}	$R_{10;-3,1}+R_{10;-13}$	$k\sqrt{2}\langle\sin 2\theta_c\sin^2\theta_d\,\mathrm{cls}(\varphi_c-2\varphi_d)\rangle$
R_{19}	$R_{10;31}-R_{10;-1,-3}$	$k\sqrt{2}\langle\sin 2\theta_c\sin 2\theta_d\cos(\varphi_c+\varphi_d)\rangle$
R_{20}	$R_{10;13}-R_{10;-3,-1}$	$k\sqrt{2}\langle\sin 2\theta_c\sin 2\theta_d\cos(\varphi_c-\varphi_d)\rangle$

The joint-decay parameters are plotted as a function of momentum transfer in Figs. 15 and 16 for the helicity frame and given in Table IV. The OPEA predictions are shown and are seen to agree with the general features of the data, at least at small momentum transfer. The experimental values are listed in Table XI of A for the individual momenta, and for the parameters as a function of t' rather than of t in Table XII of A.

A crude attempt has been made to take into account the background. Given two reactions, A and B, and two

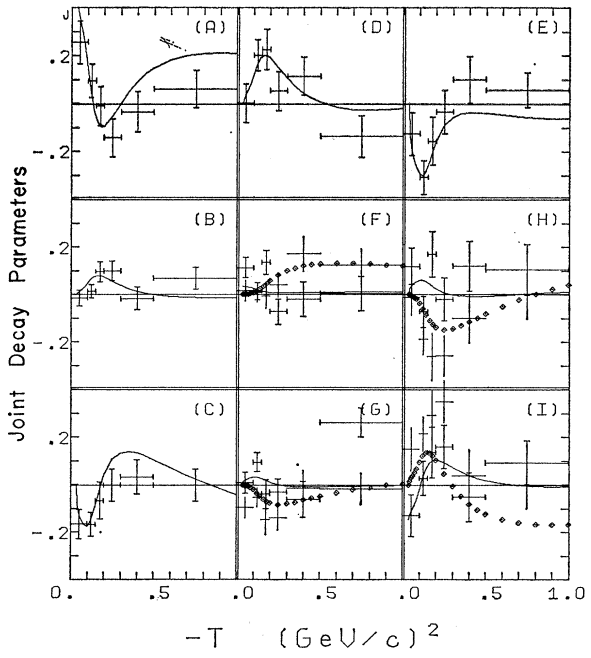

FIG. 16. $N^*\rho$ joint-decay parameters as a function of momentum transfer, with the OPEA predictions being indicated by the solid (dotted) curves, for R_8–R_{16} [(A)–(I)] using the solid curves, and R_{17}–R_{20} [(F)–(I)] using the bare errors bars and dotted curves.

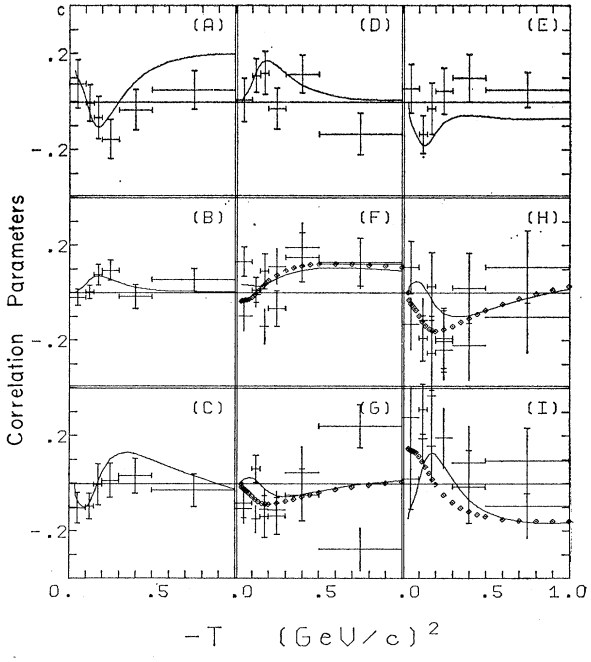

FIG. 17. $N^*\rho$ correlation parameters as a function of momentum transfer, with the OPEA predictions being indicated by the solid (dotted) curves, for C_1–C_9 [(A)–(I)] using the solid curves, and C_{10}–C_{13} [(F)–(I)] using the bare error bars and dotted curves.

TABLE IV. $N^*\rho$ decay angular distribution parameters (all momenta combined).

Parameter	$0<-t<0.1$	$0.1<-t<0.15$	$0.15<-t<0.2$	$0.2<-t<0.3$	$0.3<-t<0.5$	$0.5<-t<1.0$
			(Helicity frame)			
$\rho_{0,0}{}^c$	0.791±0.044	0.690±0.036	0.608±0.049	0.558±0.048	0.323±0.054	0.295±0.047
$\rho_{1,-1}{}^c$	−0.016±0.028	−0.054±0.024	−0.150±0.035	−0.138±0.034	−0.217±0.041	0.056±0.044
$\rho_{1,0}{}^c$	0.117±0.025	0.192±0.020	0.229±0.031	0.177±0.028	0.080±0.035	0.055±0.031
$\rho_{3,3}{}^d$	0.117±0.032	0.156±0.027	0.182±0.036	0.230±0.034	0.252±0.039	0.367±0.034
$\rho_{3,-1}{}^d$	0.003±0.030	−0.088±0.025	−0.129±0.034	−0.122±0.031	−0.004±0.039	−0.011±0.041
$\rho_{3,1}{}^d$	0.130±0.031	0.160±0.027	0.154±0.040	0.114±0.036	0.068±0.042	0.054±0.035
R_8	0.255±0.089	0.095±0.070	−0.010±0.082	−0.142±0.079	−0.034±0 083	0.062±0.078
			(Jackson frame)			
$\rho_{0,0}{}^c$	0.826±0.052	0.671±0.047	0.625±0.056	0.276±0.046	0.199±0.036	0.586±0.037
$\rho_{1,-1}{}^c$	−0.041±0.031	−0.081±0.033	−0.066±0.039	0.047±0.043	0.047±0.035	−0.000±0.026
$\rho_{1,0}{}^c$	−0.058±0.031	−0.125±0.029	−0.004±0.035	−0.054±0.032	−0.063±0.022	−0.047±0.022
$\rho_{3,3}{}^d$	0.040±0.040	0.084±0.035	0.208±0.040	0.196±0.040	0.288±0.027	0.194±0.026
$\rho_{3,-1}{}^d$	−0.047±0.032	−0.037±0.030	0.021±0.039	0.088±0.036	0.036±0.030	0.024±0.025
$\rho_{3,1}{}^d$	0.012±0.036	0.008±0.036	−0.036±0.041	−0.075±0.035	−0.074±0.028	0.018±0.026
R_8	0.435±0.120	0.393±0.091	0.110±0.103	0.154±0.084	0.082±0.058	0.212±0.066

mass regions 1 and 2, with $N_i{}^\alpha$ the number of events in region i of reaction α and $\rho_i{}^\alpha$ a density-matrix element corresponding to these events, then

$$N_1\rho_1=N_1{}^A\rho_1{}^A+N_1{}^B\rho_1{}^B, \quad N_1=N_1{}^A+N_1{}^B$$

$$N_2\rho_2=N_2{}^A\rho_2{}^A+N_2{}^B\rho_2{}^B, \quad N_2=N_2{}^A+N_2{}^B$$

$$\rho^A=\frac{N_1\rho_1N_2{}^B-N_2\rho_2N_1{}^B}{N_1{}^AN_2{}^B-N_2{}^AN_1{}^B} \quad \left(\text{for } \frac{N_1{}^A}{N_1{}^B}\neq\frac{N_2{}^A}{N_2{}^B}\right)$$

$$\rho^A=\frac{\beta_2\rho_1-\beta_1\rho_2}{\alpha_1\beta_2-\alpha_2\beta_1}, \quad \alpha_i=\frac{N_i{}^A}{N_i}, \quad \beta_i=1-\alpha_i.$$

Corrected density-matrix elements have been calculated using this formula, with A being $N^*\rho$ production, B being the background, and taking the relative fraction of each from the fit to the triangle plot. These are listed in Table V. This correction is seen not to alter materially the density-matrix elements. Since the matrix elements are functions of the resonance masses, the differences between the "corrected" and "uncorrected" values may be largely a consequence of their being obtained in different mass regions. This is particularly true because of the large component of $N^*\rho$ "tail" in the background region.

It was noted several years ago[10] that the decays of

TABLE V. $N^*\rho$-decay angular distribution parameters, corrected for background (all momenta combined).

Parameter	$0<-t<0.1$	$0.1<-t<0.15$	$0.15<-t<0.2$	$0.2<-t<0.3$	$0.3<-t<0.5$	$0.5<-t<1.0$
$\rho_{0,0}{}^c$	0.896±0.082	0.676±0.065	0.547±0.086	0.467±0.084	0.259±0.095	0.266±0.084
$\rho_{1,-1}{}^c$	−0.008±0.051	−0.028±0.045	−0.166±0.062	−0.146±0.060	−0.253±0.072	0.104±0.077
$\rho_{1,0}{}^c$	0.175±0.048	0.247±0.041	0.246±0.054	0.136±0.050	−0.023±0.062	−0.029±0.054
$\rho_{3,3}{}^d$	0.039±0.060	0.185±0.049	0.183±0.063	0.254±0.059	0.293±0.068	0.367±0.062
$\rho_{3,-1}{}^d$	0.016±0.053	−0.122±0.046	−0.126±0.060	−0.130±0.055	0.004±0.067	0.027±0.071
$\rho_{3,1}{}^d$	0.150±0.056	0.175±0.048	0.137±0.068	0.092±0.062	0.020±0.073	0.019±0.062
R_8	0.359±0.157	0.061±0.129	−0.137±0.146	−0.294±0.137	−0.119±0.148	0.096±0.140
R_9	−0.050±0.061	−0.035±0.054	0.169±0.077	0.150±0.075	−0.110±0.084	0.097±0.083
R_{10}	−0.272±0.113	−0.232±0.096	−0.073±0.138	0.013±0.119	0.074±0.124	−0.108±0.117
R_{11}	−0.065±0.143	0.292±0.118	0.239±0.149	−0.033±0.145	0.172±0.137	−0.159±0.154
R_{12}	−0.035±0.159	−0.385±0.130	−0.092±0.170	0.140±0.154	0.125±0.173	0.107±0.130
R_{13}	0.249±0.086	0.034±0.067	0.170±0.092	−0.135±0.095	−0.084±0.126	−0.015±0.128
R_{14}	−0.024±0.082	−0.018±0.070	−0.088±0.094	−0.063±0.091	0.265±0.130	0.206±0.125
R_{15}	−0.025±0.081	0.104±0.074	−0.041±0.106	−0.069±0.096	−0.023±0.130	0.390±0.112
R_{16}	−0.087±0.080	−0.069±0.074	−0.233±0.109	−0.212±0.095	0.010±0.134	−0.051±0.116
R_{17}	0.193±0.141	−0.215±0.126	0.448±0.185	0.004±0.158	0.166±0.180	0.274±0.188
R_{18}	0.033±0.140	−0.367±0.129	−0.353±0.178	−0.342±0.152	−0.122±0.176	0.019±0.178
R_{19}	−0.200±0.157	0.075±0.131	0.165±0.185	0.206±0.154	−0.234±0.179	0.270±0.167
R_{20}	0.082±0.159	0.322+0.134	0.320±0.182	0.460±0.152	−0.017±0.191	0.010±0.171
			(Jackson frame)			
$\rho_{0,0}{}^c$	0.956±0.081	0.884±0.064	0.808±0.090	0.594±0.082	0.554±0.095	0.243±0.083
$\rho_{1,-1}{}^c$	0.023±0.048	0.076±0.044	−0.036±0.055	−0.082±0.057	−0.106±0.069	0.093±0.076
$\rho_{1,0}{}^c$	0.006±0.049	−0.016±0.042	−0.033±0.055	−0.115±0.052	0.069±0.061	0.006±0.055
$\rho_{3,3}{}^d$	−0.009±0.059	0.043±0.049	0.058±0.069	0.110±0.061	0.256±0.070	0.245±0.070
$\rho_{3,-1}{}^d$	0.043±0.050	−0.040±0.042	−0.054±0.057	−0.048±0.052	0.025±0.066	0.097±0.064
$\rho_{3,1}{}^d$	−0.028±0.060	0.059±0.051	−0.024±0.066	0.013±0.063	−0.011±0.071	−0.065±0.062
R_8	0.387±0.161	0.556±0.137	0.337±0.204	0.409±0.154	−0.041±0.177	0.209±0.152

the N^{*++} and ρ^0 were not independent, but that the ρ^0-decay cosine distribution was different for different regions of the N^*-decay cosine and vice versa. The explanation of these correlations has been one of the major successes of the OMEA model.

In general, for a joint distribution $W(\theta_c,\varphi_c;\theta_d,\varphi_d)$ no correlation between the two decays occurs if the joint distribution factors into a product of individual distributions:

$$W(\theta_c,\varphi_c;\theta_d,\varphi_d)=W_c(\theta_c,\varphi_c)W_d(\theta_d,\varphi_d). \quad (13)$$

The $N^*\rho$ joint distribution is of the form

$$W=k(1+\sum_i A_i^c f_i^c+\sum_i A_i^d f_i^d+\sum_{ij} B_{ij} f_i^c f_j^d + \sum_k A_k f_k)(\theta_c,\varphi_c;\theta_d,\varphi_d) \quad (i,j=1,3;k=4,7), \quad (14)$$

where the A_i^α and B_{ij} are functions of the decay parameters and the f_i are orthogonal functions of the relevant angles:

$$f_1(\theta,\varphi)=1-3\cos^2\theta, \quad f_2(\theta,\varphi)=\sin^2\theta\cos 2\varphi,$$
$$f_3(\theta,\varphi)=\sin 2\theta\cos\varphi,$$
$$f_4(\theta_c,\varphi_c;\theta_d,\varphi_d)=\sin^2\theta_c\sin^2\theta_d\sin 2\varphi_c\sin 2\varphi_d,$$
$$f_5=\sin^2\theta_c\sin 2\theta_d\sin 2\varphi_c\sin\varphi_d,$$
$$f_6=\sin 2\theta_c\sin^2\theta_d\sin\varphi_c\sin 2\varphi_d,$$
$$f_7=\sin 2\theta_c\sin 2\theta_d\sin\varphi_c\sin\varphi_d.$$

From (13) and (14) the conditions which must hold if there are to be no correlations are obvious:

$$B_{ij}-A_i^c A_j^d=0, \quad i,j=1,3$$
$$A_k=0, \quad k>3.$$

The above 13 equations determine a set of correlation parameters, whose divergence from zero would indicate the presence of decay correlations. More explicitly,

$$A_1^c=\tfrac{1}{2}(1-3\rho_{00}^c), \quad A_1^d=-\tfrac{1}{2}(1-4\rho_{33}^d),$$
$$A_2^c=-3\rho_{1,-1}^c, \quad A_2^d=-2\sqrt{3}\rho_{3,-1}^d,$$
$$A_3^c=-3\sqrt{2}\rho_{1,0}^c, \quad A_3^d=-2\sqrt{3}\rho_{3,1}^d,$$

and the correlation parameters are defined as follows:

$$C_1=R_8-A_1^c A_1^d,$$
$$C_2=R_9+\tfrac{1}{3}A_2^c A_1^d,$$
$$C_3=R_{10}+\tfrac{1}{3}A_3^c A_1^d\sqrt{2},$$
$$C_4=R_{11}+A_1^c A_2^d/\sqrt{3},$$
$$C_5=R_{12}+A_1^c A_3^d/\sqrt{3},$$
$$C_6=(R_{13}+R_{14})-A_2^c A_2^d/(3\sqrt{3}),$$
$$C_7=(R_{15}+R_{16})-A_2^c A_3^d/(3\sqrt{3}),$$
$$C_8=(R_{17}+R_{18})-A_3^c A_2^d\sqrt{2}/(3\sqrt{3}),$$
$$C_9=(R_{19}+R_{20})-A_3^c A_3^d\sqrt{2}/(3\sqrt{3}),$$

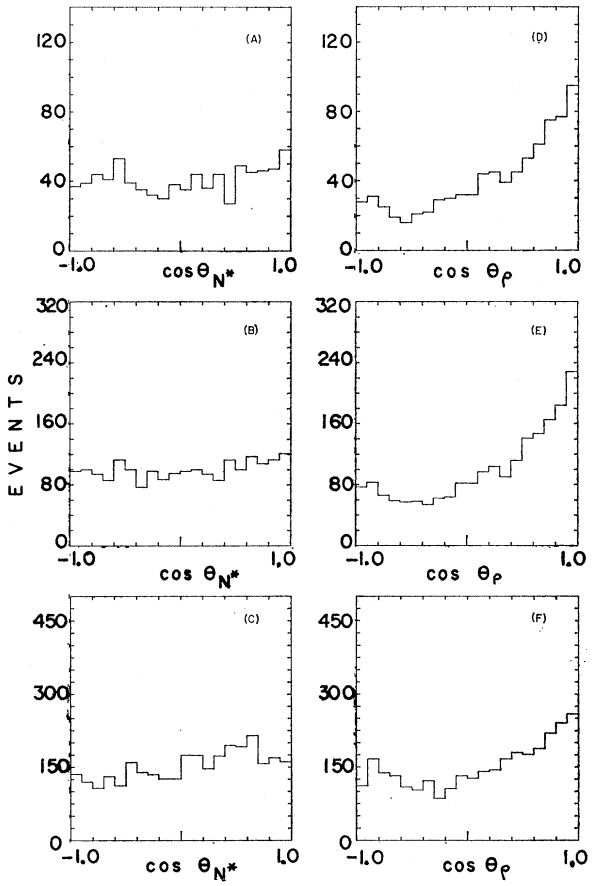

FIG. 18. N^* (left) and ρ (right) decay cosine distributions for the three following mass regions: central $N^*\rho$—(A) and (D), $N^*\rho$ region—(B) and (E), background region—(C) and (F).

$$C_{10}=R_{14}-R_{13},$$
$$C_{11}=R_{16}-R_{15},$$
$$C_{12}=R_{18}-R_{17},$$
$$C_{13}=R_{20}-R_{19}.$$

These parameters are listed in Table XIV of A for each momentum and are shown in Fig. 17 for the combined data. The OPEA predictions are again superimposed on the data and agree rather well with them. It is especially noteworthy that experiment and theory are in reasonable agreement for the $\cos\theta_\rho$–$\cos\theta_{N^*}$ correlation, since this is the most prominent of the correlations.

In all of the above, no provision is made for any asymmetry in the $\cos\theta_\rho$ or $\cos\theta_{N^*}$ distributions. Given the general formula for the joint-decay distribution no such asymmetry is permissible. It is well known, however, that such an asymmetry not only exists for ρ meson but is very large.[10] Figure 18 shows the $\cos\theta_\rho$ (and $\cos\theta_{N^*}$) distributions for $N^*\rho$ events. The figure also shows these distributions for a tight $N^*\rho$ cut and for a background sample. The magnitude of the effect is seen by noting that the forward-to-backward

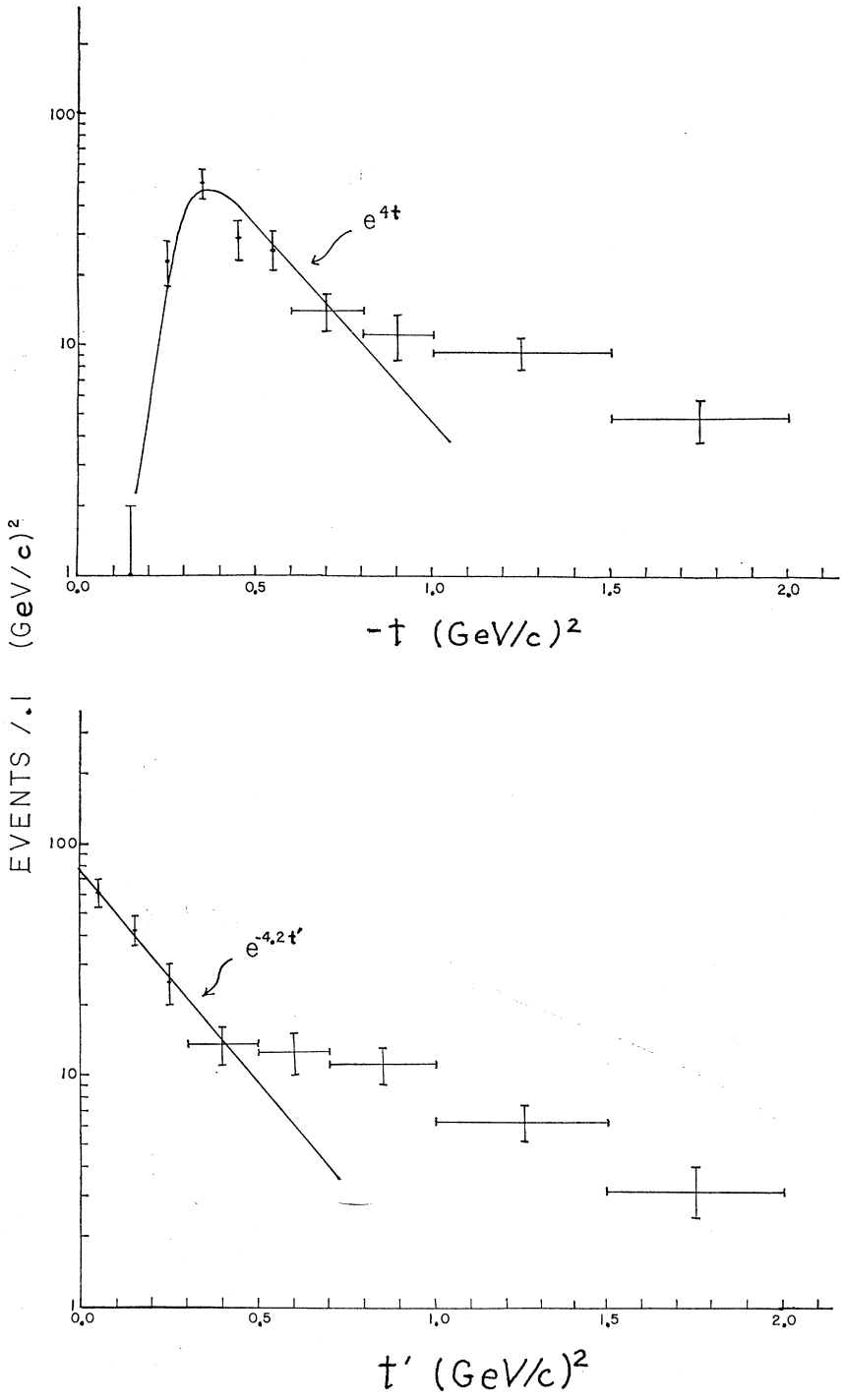

FIG. 19. N^*f $-t$ and t' distributions for the events of the highest three momenta combined.

ratio $(F/B)_\rho$ for the $N^*\rho$ region is 2.3, implying a 30% excess of events in the forward direction. That the effect is associated with $N^*\rho$ production is confirmed by the fact that the effect is heightened in the central $N^*\rho$ region and diminished in the background region. Using the method of moments to obtain the decay parameters from formula (13) effectively involved folding the distribution about $\theta=\frac{1}{2}\pi$ and ignoring the asymmetry.

B. $\pi^+p \rightarrow N^{*++}f^0$

N^*f production is evident at the three highest momenta. At those energies it accounts for from 3.6 to

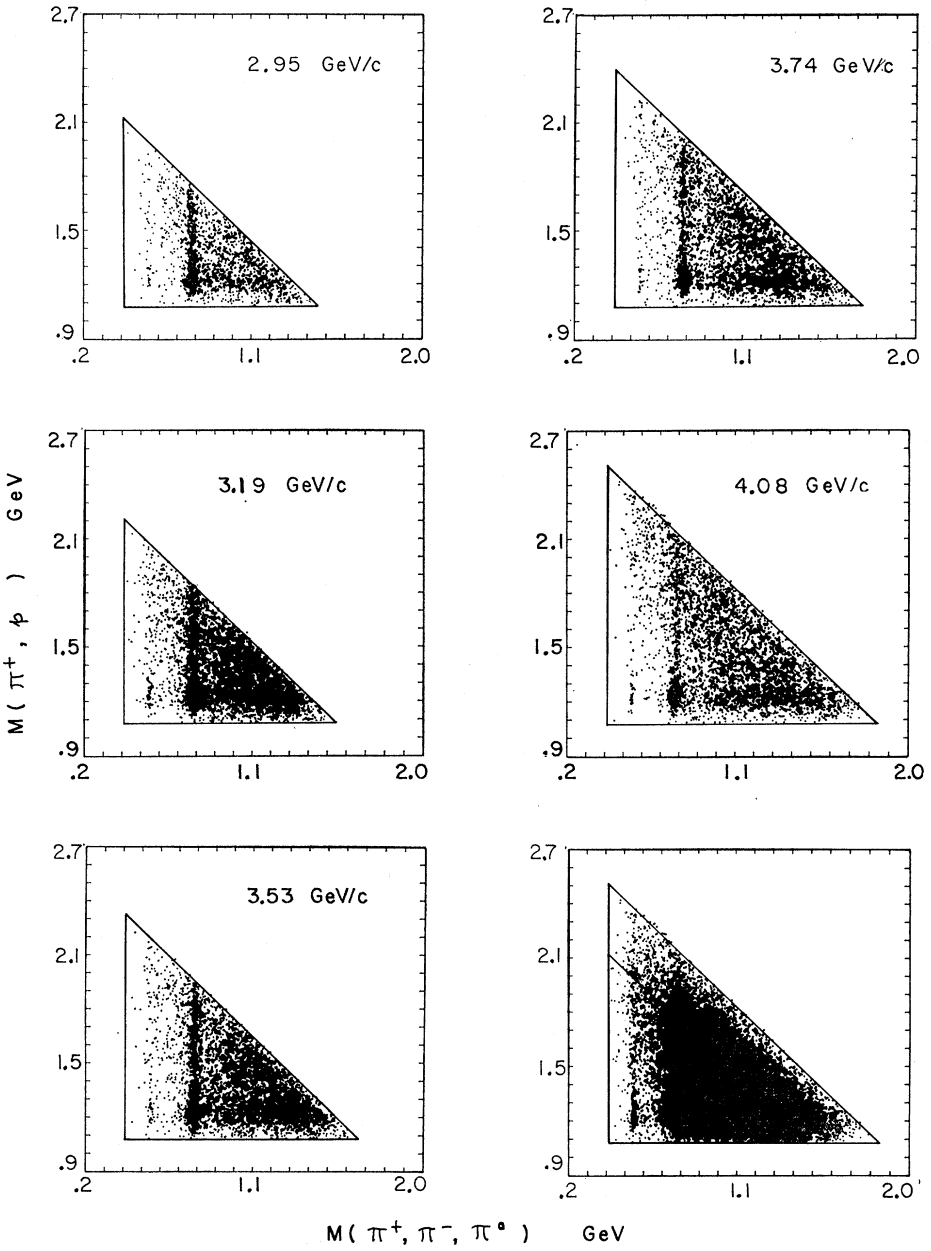

FIG. 20. π^+p–$\pi^+\pi^-\pi^0$ triangle plots for reaction (2) for the individual momenta and their sum. Both combinations are plotted for each event.

5.9% of reaction (1), according to the fit of the $\pi^+\pi^-$–π^+p triangle plot. Its cross section has already been presented in Fig. 10. The event sample consisted of 312 events selected from the upper three momenta.

The N^*f cuts are as follows: $1.17<M(\pi^+\pi^-)<1.31$, $1.12<M(\pi^+p)<1.32$ GeV, with the usual stipulation that double-N^*f events are decided on the basis of the lower momentum transfer. An additional requirement was added in order to discriminate against $N^*\rho$ events. Neither of the π^+p, $\pi^+\pi^-$ combinations was permitted to lie within the $N^*\rho$ region, as previously defined.

The background problem was quite severe. Using the above selection criteria it was estimated to be about 55, 53, and 41% at the three momenta. Therefore, considerable reliance is henceforward placed upon the background calculation outlined in Sec. III A. The outer limits on the background region for this calculation were set to be as follows: $1.08<M(\pi^+\pi^-)<1.40$ GeV, $1.02<M(\pi^+p)<1.42$ GeV.

The proximity of the N^*f region to the kinematic boundary renders a simple fit to the $-t$ forward peak impossible. The boundary region extends to $-t=0.64$ $(\text{GeV}/c)^2$, with the mass cuts used, and thus encompasses almost the entire forward region. This gives us

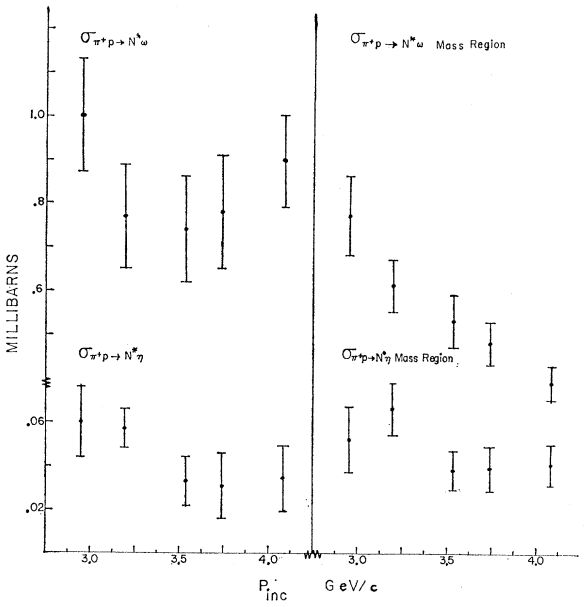

FIG. 21. Cross sections for $N^*\omega$ and $N^*\eta$ production from the fit to the triangle plot, and for production of events within the $N^*\omega$ and $N^*\eta$ mass regions—i.e., of events with $0.75<M(\pi_i^+\pi^-\pi^0)<0.81$ GeV/c^2 for ω, $0.53<M(\pi_i^+\pi^-\pi^0)<0.57$ GeV/c^2 for η, and $1.12<M(\pi_j^+\rho)<1.32$ GeV/c^2.

limited sensitivity to the very peripheral events and probably accounts for the relatively flat energy dependence of the N^*f cross section. The value $A\simeq 4$ was obtained from a rough comparison of the t distribution with Monte Carlo events. A fit to the t' distribution, yielded $A=4.21\ \pm 0.43$ (GeV/c)$^{-2}$. The distribution is much more highly peaked at the highest momentum [$A=7.1\pm 0.5$ (GeV/c)$^{-2}$] than at the other two. ($A=2.5\pm 0.8$ and 2.9 ± 0.9.) The $-t$ and t' distributions are displayed in Fig. 19 together with curves representing the above-mentioned exponential dependences.

C. $\pi^+p\rightarrow N^{*++}\omega^0$

$N^*\omega$ production accounts for about 20% of reaction (2). The fit to the $\pi^+\pi^-\pi^0$–π^+p triangle plot (Fig. 20) was less ambitious than that described previously for reaction (1). Because of the greater uncertainty in what processes might be contributing to the background, characteristics not immediately recognizable in the $\pi^+\pi^-\pi^0$–π^+p triangle plot were ignored. The Monte Carlo program was used to generate events according to the following six final states:

$$\pi^+p\rightarrow\pi^+p\pi^+\pi^-\pi^0 \text{ (phase space)} \quad (15)$$

$$\rightarrow N^{*++}\pi^+\pi^-\pi^0\ (e^t) \quad (16)$$

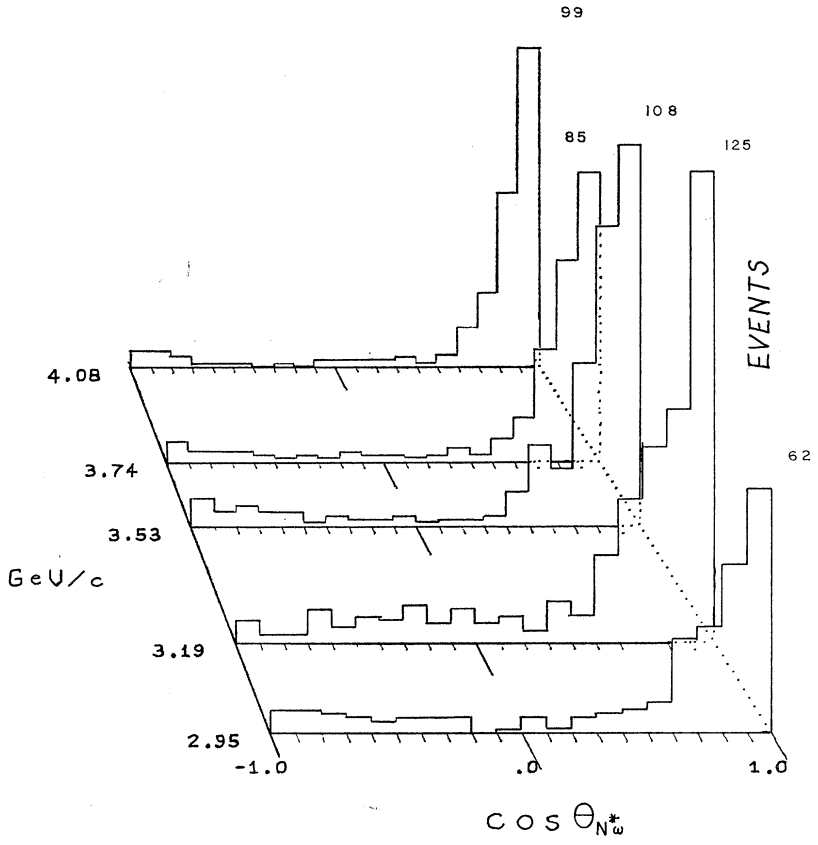

FIG. 22. $N^*\omega$-production cosine distributions at the five momenta. The numbers of events in the last bins are indicated.

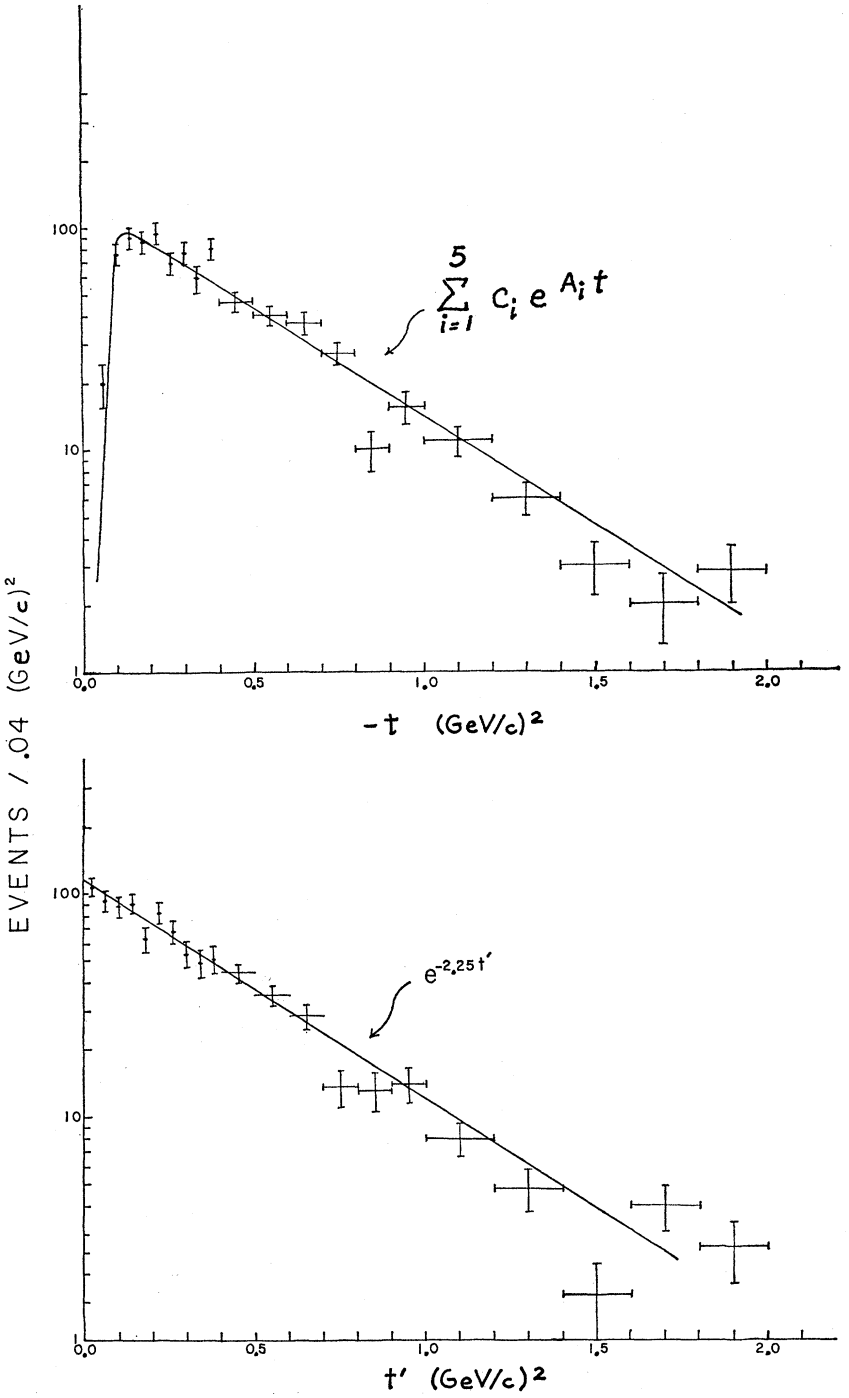

FIG. 23. $N^*\omega$ $-t$ and t' distributions. The upper curve is the sum of curves at each momentum, using the logarithmic slopes of Table VI.

$$\pi^+p \rightarrow N^{*++}\omega^0 \ (e^{3t}) \tag{17}$$

$$\rightarrow \pi^+p\omega^0 \ (e^{t}) \tag{18}$$

$$\rightarrow N^{*++}\eta^0 \ (e^{3t}) \tag{19}$$

$$\rightarrow \pi^+p\eta^0 \ (e^{t}). \tag{20}$$

The procedure is that previously used, except that for the ω and η it was not sufficient to use the Particle Data Group's[21] resonance parameters, because the experimental resolution was large in comparison with the real widths. In a fit to the $M(\pi^+\pi^-\pi^0)$ distribution, values of 25.5±1.3 MeV and 20.6±34.6 MeV were obtained for the ω and η widths, respectively, yielding ~22 MeV for the experimental mass resolution.

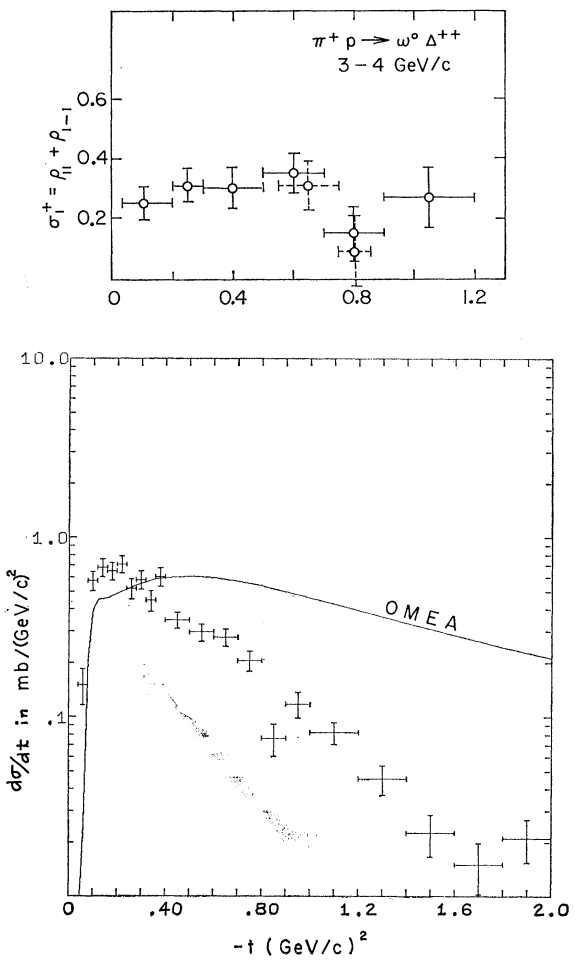

FIG. 24. $\rho_{11}+\rho_{1-1}$ and $d\sigma/dt$ for $N^*\omega$ production in the $N^*\omega$ mass region. For $d\sigma/dt$, the solid curve is the OMEA prediction (×4.0).

The resultant $N^*\omega$ and $N^*\eta$ cross sections are plotted in Fig. 21. Because of the uncertainty in the background parametrization the fitted cross sections are much less reliable than for the case of $N^*\rho$ production.

The $N^*\omega$ mass region was chosen to lie within the bounds $0.75<M(\pi^+\pi^-\pi^0)<0.81$ GeV, $1.12<M(\pi^+p)<1.32$ GeV. Again, double-$N^*\omega$ ambiguities were resolved on the basis of the lower momentum transfer.

TABLE VI. Logarithmic slopes of the $-t$ and t' distributions in $N^*\omega$ production. [$0.2<-t<1.2$ (GeV/c)^2, $0.0<t'<1.0$ (GeV/c)^2.]

Momentum (GeV/c)	$A_{N^*\omega}{}^{-t}$ (GeV/c)$^{-2}$	$A_{N^*\omega}{}^{t'}$ (GeV/c)$^{-2}$
2.95	2.16±0.25	2.54±0.14
3.19	2.05±0.19	2.14±0.17
3.53	2.15±0.17	2.06±0.15
3.74	2.45±0.22	2.12±0.18
4.08	2.71±0.28	2.59±0.20
Combined	2.31±0.06	2.25±0.08

Since this reaction is less peripheral than $N^*\rho$ production, choosing the correct combination on the basis of the lower $-t_{p,N^*}$ is of less validity than before. It is an improvement over picking one of the combinations at random or averaging the two, however. As was seen in Fig. 8, choosing the combination with the lower $-t_{p,N^*}$ clearly enhances the N^* and ω signals. This affects only 1.1% of the events, fortunately.

Comparisons will again be made between the experimental results and predictions of the OMEA. This model will be seen to be in rather poor agreement with experiment.

The production cosine distribution is shown in Fig. 22. The usual forward peak is in evidence, but much less steep than for $N^*\rho$ production, and with only 34% of the events having $\cos\theta>0.9$. Also, there is a distinct backward peak, less than 10% of the forward peak in magnitude, but definitely not merely a statistical fluctuation. It becomes more noticeable as the momentum is increased and the equatorial zone becomes denuded of events.

The momentum-transfer distribution is shown in Fig. 23. It is much less steeply peaked than was the corresponding $N^*\rho$ distribution. The peak was fitted to an exponential and found to have a logarithmic slope of 2.31±0.06 (GeV/c)$^{-2}$ over the interval $0.2<t<1.2$ (GeV/c)^2. The $N^*\omega$ distribution has a simple exponential behavior over a much wider range of $-t$ than did the $N^*\rho$ distribution, and in particular lacks the $N^*\rho$'s anomalous behavior in the boundary region. Looking at Figs. 12 and 23, it is interesting to note that whereas the $N^*\rho$ distribution is "concave"—i.e., has a slope which decreases with increasing $-t$—the $N^*\omega$ distribution appears to be even slightly convex, at least up to about $-t=1.5$ (GeV/c)^2. There also appears to be some evidence for a dip at $-t=0.8$ (GeV/c)^2.

The t' distribution (Fig. 23) was also fitted to an exponential. The resultant slope, for the interval $0<t'<1$ (GeV/c)^2, was $A_{N^*\omega}{}^{t'}=2.25\pm0.08$ (GeV/c)$^{-2}$.

The fitted values of the slopes for t and t' are given in Table VI for each momentum separately. The values for the momentum transfer seem to indicate a definite shrinkage of the peak (increase in A) with energy.

In order to properly normalize the momentum-transfer distribution, the same procedure employed for the $N^*\rho$ was used. The background values for $N^*\omega$ (and $N^*\eta$) regions were used in conjunction with the mb/event figures of Table I to obtain $d\sigma/dt$.

$d\sigma/dt$ is shown in Fig. 24 along with the OMEA predictions mutliplied by a factor of 4. The OMEA curve is seen to bear little resemblance to the experimental distribution. The scale factor of 4, needed to normalize to the data peak, could be obtained by increasing the coupling constants and/or increasing the value of the absorption parameter γ_f. The very shallow slope of the curve would not be greatly affected by either of these expedients; however, there are three coupling con-

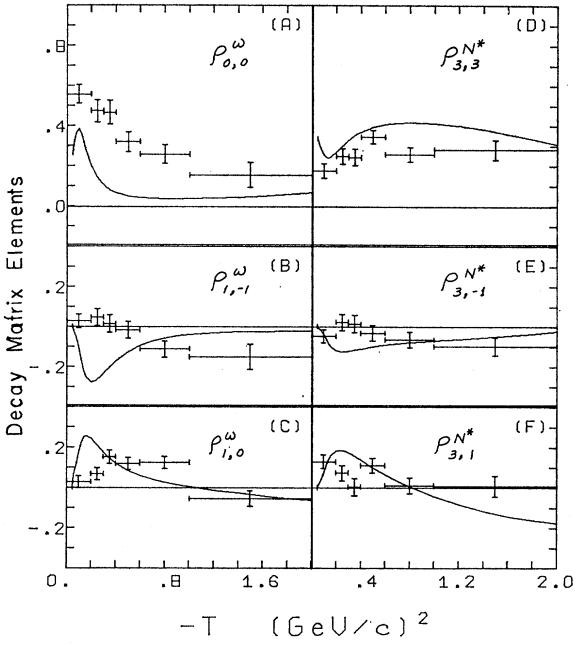

FIG. 25. $N^*\omega$-decay matrix elements as a function of momentum transfer, with the OMEA predictions being indicated by the solid line, for (A) $\rho_{0,0}{}^{\omega}$, (B) $\rho_{1,-1}{}^{\omega}$, (C) $\rho_{1,0}{}^{\omega}$, (D) $\rho_{3,3}{}^{N^*}$, (E) $\rho_{3,-1}{}^{N^*}$, (F) $\rho_{3,1}{}^{N^*}$.

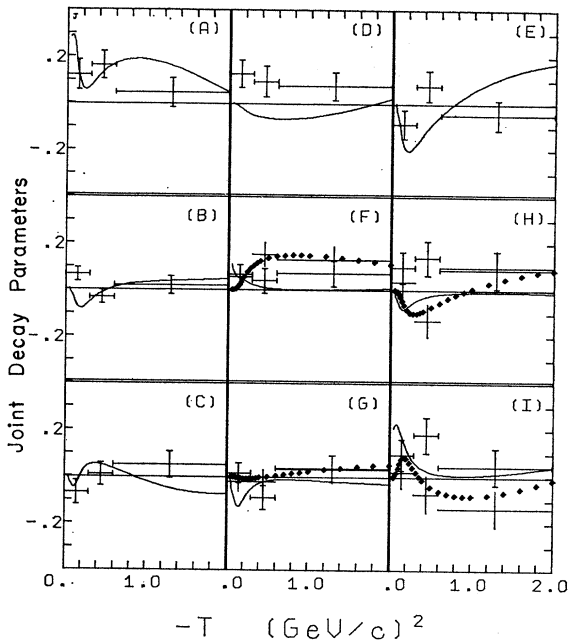

FIG. 26. $N^*\omega$ joint-decay parameters as a function of momentum transfer, with the OMEA predictions being indicated, for R_8–R_{16} [(A)–(I)] with the solid curve, and R_{17}–R_{20} [(F)–(I)] with the bare error bars and dotted curve.

stants at the $N^{*++}\rho p$ vertex, and changing the ratios of these could effect the slope of $d\sigma/dt$. At least with the usual (relativistic Stodolsky-Sakurai) coupling, the ρ-exchange model, even with absorption, is seen to be in serious difficulty. Further, the Regge model with exchange of the ρ trajectory predicts a dip in $d\sigma/dt$ at $-t\simeq 0.55$ (GeV/c)^2.[24] There being no evidence in our data for such a dip, the validity of the pure ρ-exchange mechanism is again brought into question, and some addition, such as B exchange, has been proposed.

Several attempts have been made to extract the ρ-exchange contribution for reaction (2).[25] In particular, the asymptotic relation $\rho_{1-1}=-\rho_{11}$ should be satisfied at the value of t where the ρ-exchange contribution vanishes or, more practically, the combination $\sigma_1{}^+\equiv\rho_{11}+\rho_{1-1}$ should exhibit a minimum. In Fig. 24 we show $d\sigma/dt(t)$ and $\sigma_1{}^+(t)$ for our data. While no dip is observed at $t=-0.5$, we note a suggestion of a dip at $t=0.8$ in both distributions. Such a dip also seems to occur in the data of Alff-Steinberger *et al.*[26] between 2.3 and 2.9 GeV/c incident momentum. In no single distribution is the dip statistically significant, but its recurrence suggests further experiments.

The angular decay parameters are treated for the $N^*\omega$ in precisely the same manner as they were for the $N^*\rho$. The only important distinction between the two cases is that the vector of interest in the meson-decay

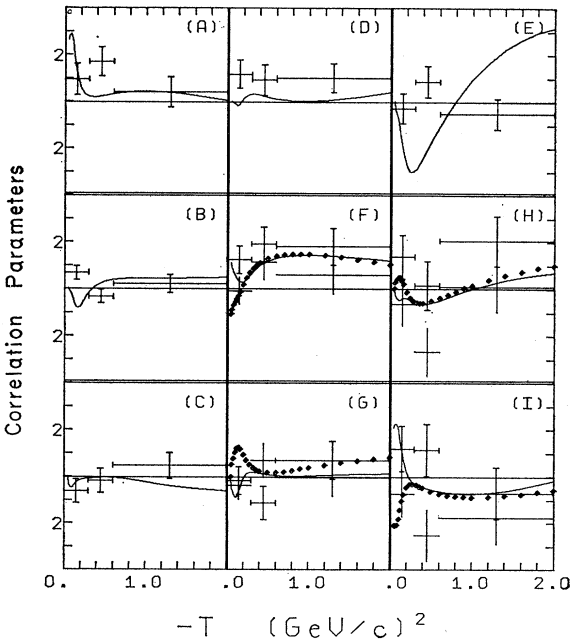

FIG. 27. $N^*\omega$ correlation parameters as a function of momentum transfer, with the OMEA prediction being indicated, for C_1–C_9 [(A)–(I)] with the solid curve, and C_{10}–C_{13} [(F)–(I)] with the bare error bars and dotted curve.

[24] F. Arbab and C. B. Chiu, Phys. Rev. **147**, 1045 (1966).
[25] H. Högaasen and H. J. Lubatti, Phys. Letters **26B**, 166 (1968); J. P. Ader, M. Capdeville, G. Cohen-Tannoudji, and Ph. Salin, Nuovo Cimento **56A**, 962 (1968).
[26] C. Alff-Steinberger, D. Berley, D. Colley, N. Gelfand, D. Miller, U. Nauenberg, J. Schultz, T. H. Tan, H. Brugger, P. Kramer, and R. Plano, Phys. Rev. **145**, 1072 (1966); N. Gelfand (Ref. 6).

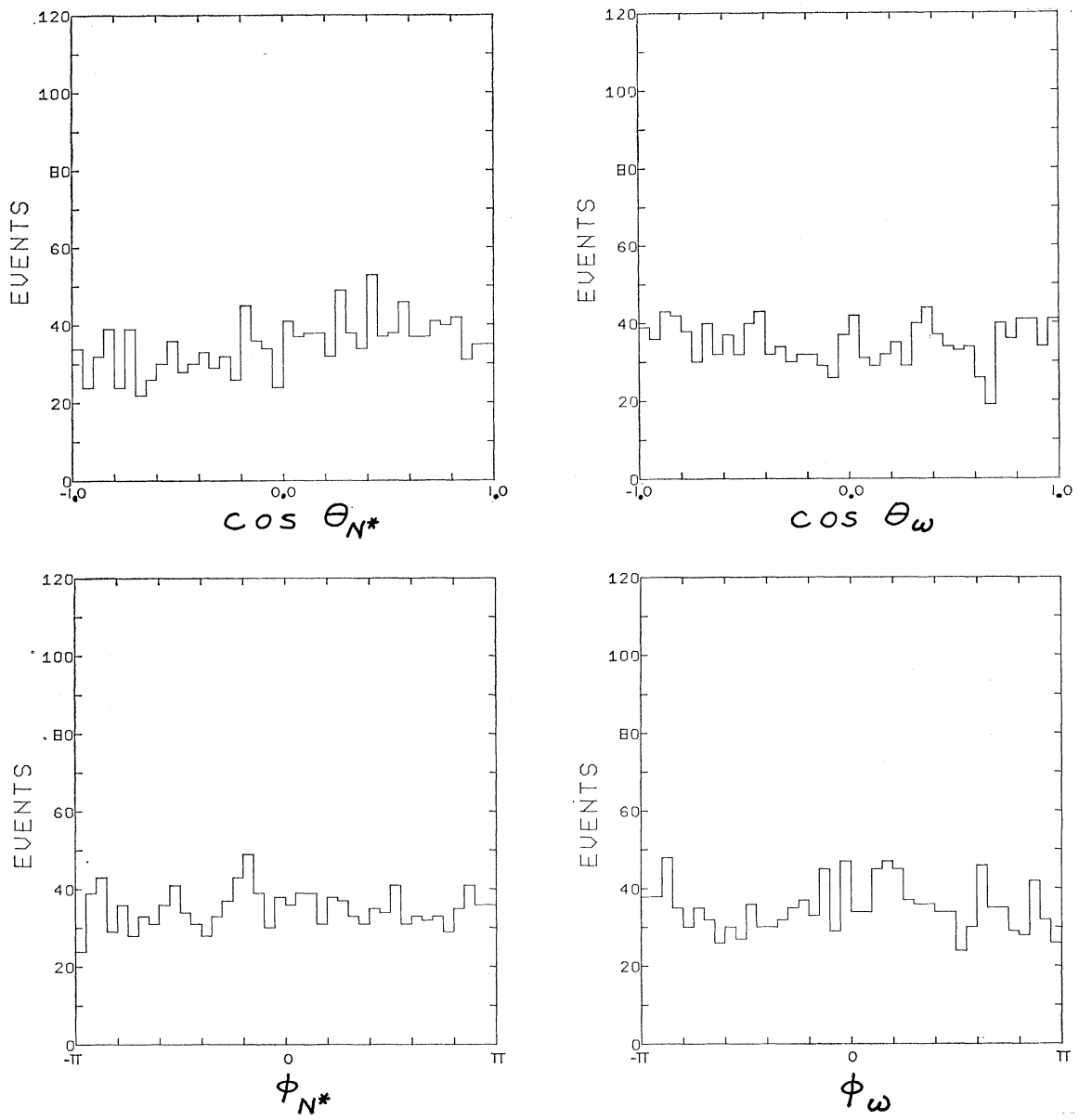

FIG. 28. N^* (left) and ω (right) decay angular distributions in the helicity frame.

frame is not the direction of one of the outgoing particles—i.e., the π^+ for the ρ—but is instead the normal to the ω-decay plane. Otherwise, since the ρ and ω are both 1^- particles, the same parametrization is applicable for both the $N^*\rho$ and $N^*\omega$ systems. The decay parameters are presented in Tables XXII and XXV of A and are shown in Figs. 25–27 in the helicity frame as a function of momentum transfer.

The curves superimposed upon the data points in Figs. 25–27 are the OMEA predictions. Obviously, the theoretical predictions are not at all well borne out by this experiment. The background calculation slightly improves this situation, but not sufficiently for the model to attain any real measure of success. No satisfactory agreement was attained, moreover, in a thorough but not exhaustive variation of the vertex coupling constants.

Finally, the $\cos\theta$ and φ distributions for both the ω and N^* are shown in Fig. 28. They are all roughly isotropic. In particular the $\cos\theta_\omega$ distribution bears no trace of anything similar to the asymmetry which dominates the corresponding ρ distribution.

D. $\pi^+ p \rightarrow N^{*++}\eta^0$

$N^{*++}\eta^0$ production accounts for only a very small percent ($\sim$1.2%) of reaction (2). Because of the small

width of the η and the position of the $N^*\eta$ region near the kinematic boundary, however, a very clean sample of $N^*\eta$ events may be obtained. The mass-selection criteria require $0.53<M(\pi^+\pi^-\pi^0)<0.57$ GeV, $1.12<M(\pi^+p)<1.32$ GeV, with no combination allowed in the $N^*\omega$ region, and ambiguities resolved on the basis of the smaller momentum transfer. For these criteria the background is at about the 20% level.

Since only 124 events pass the above $N^*\eta$ criteria, the different momenta are not considered separately; the $-t$, t', and $\cos\theta_{N^*\eta}$ distributions and the N^{*++} decay parameters are given only for the experiment as a whole.

The t and t' distributions are shown in Fig. 29. Because the boundary region extends only to $-t=0.67$ $(\mathrm{GeV}/c)^2$, they are practically identical. They are very different from those previously encountered. Of the four double-resonance reactions studied, this is the only one with a turnover in the t' distribution. Neither remotely resembles an exponential distribution, so no logarithmic slope parameter A was obtained.

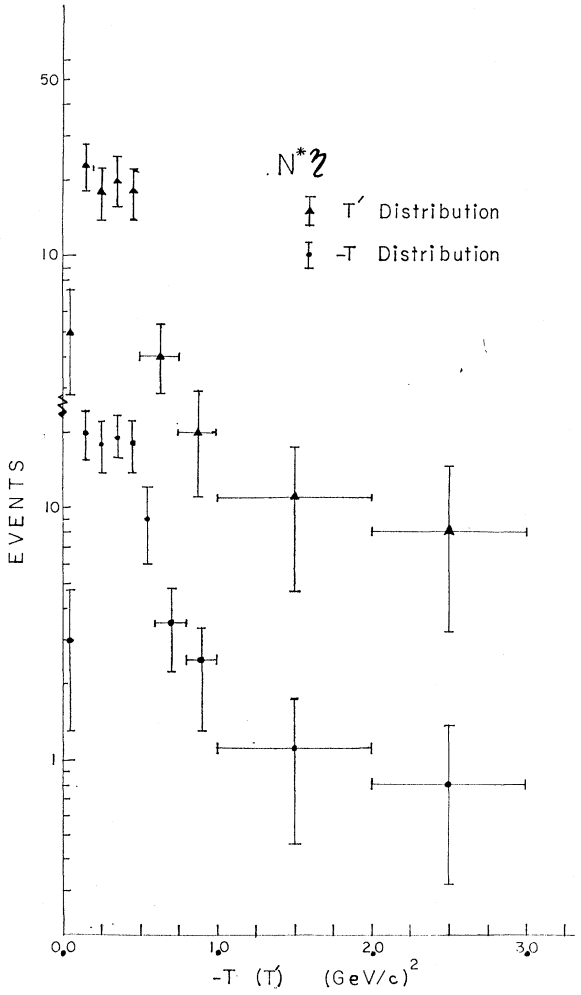

FIG. 29. $N^*\eta$ $-t$ and t' distributions.

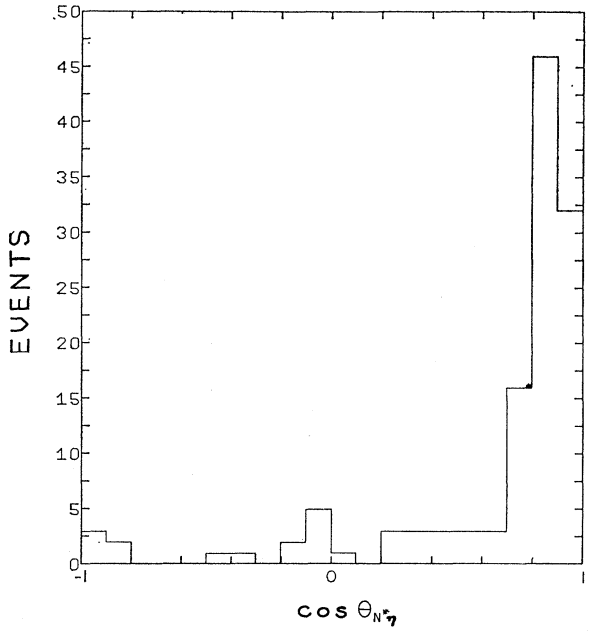

FIG. 30. $N^*\eta$-production cosine distribution.

The $\cos\theta_{N^*\eta}$ distribution (Fig. 30) further demonstrates the anomolous behavior of the forward peak. Not only do fewer than 26% of the events lie beyond $\cos\theta=0.9$, there are actually over 40% more events in the neighboring $\cos\theta$ bin ($0.8<\cos\theta_{N^*}<0.9$). Most of the events are, however, concentrated in the forward direction, although there is some indication of a backward peak as well.

The decay angular distributions (helicity frame) are shown in Fig. 31, and the N^* decay parameters are listed below. The decay distributions are roughly compatible with isotropy with one exception. The exception is the $\cos\theta_{N^*}$ distribution, which displays a striking peak around $\theta=\frac{1}{2}\pi$. The N^* decay parameters are as follows:

$$\rho_{3,3}{}^d=0.435\pm0.044,\ 0.455\pm0.052 \quad (0.441\pm0.068,\ 0.507\pm0.088),$$

$$\rho_{3,-1}{}^d=0.202\pm0.054,\ 0.221\pm0.067 \quad (0.282\pm0.088,\ 0.340\pm0.113),$$

$$\rho_{3,1}{}^d=-0.008\pm0.042,\ -0.008\pm0.052 \quad (-0.001\pm0.066,\ 0.059\pm0.093),$$

where the background-corrected parameters are given in parentheses, and the second member of each pair is for the region $-t<0.5$ $(\mathrm{GeV}/c)^2$. The value of $\rho_{3,3}{}^d$ is a measure of the deviation of the $\cos\theta_{N^*}$ distribution from isotropy, being roughly that for a $\sin^2\theta$ distribution (0.5) and nearly twice that of an isotropic distribution (0.25). These results are in agreement with A_2-pole exchange predictions.[27]

[27] M. Krammer, Nuovo Cimento **52A**, 931 (1967).

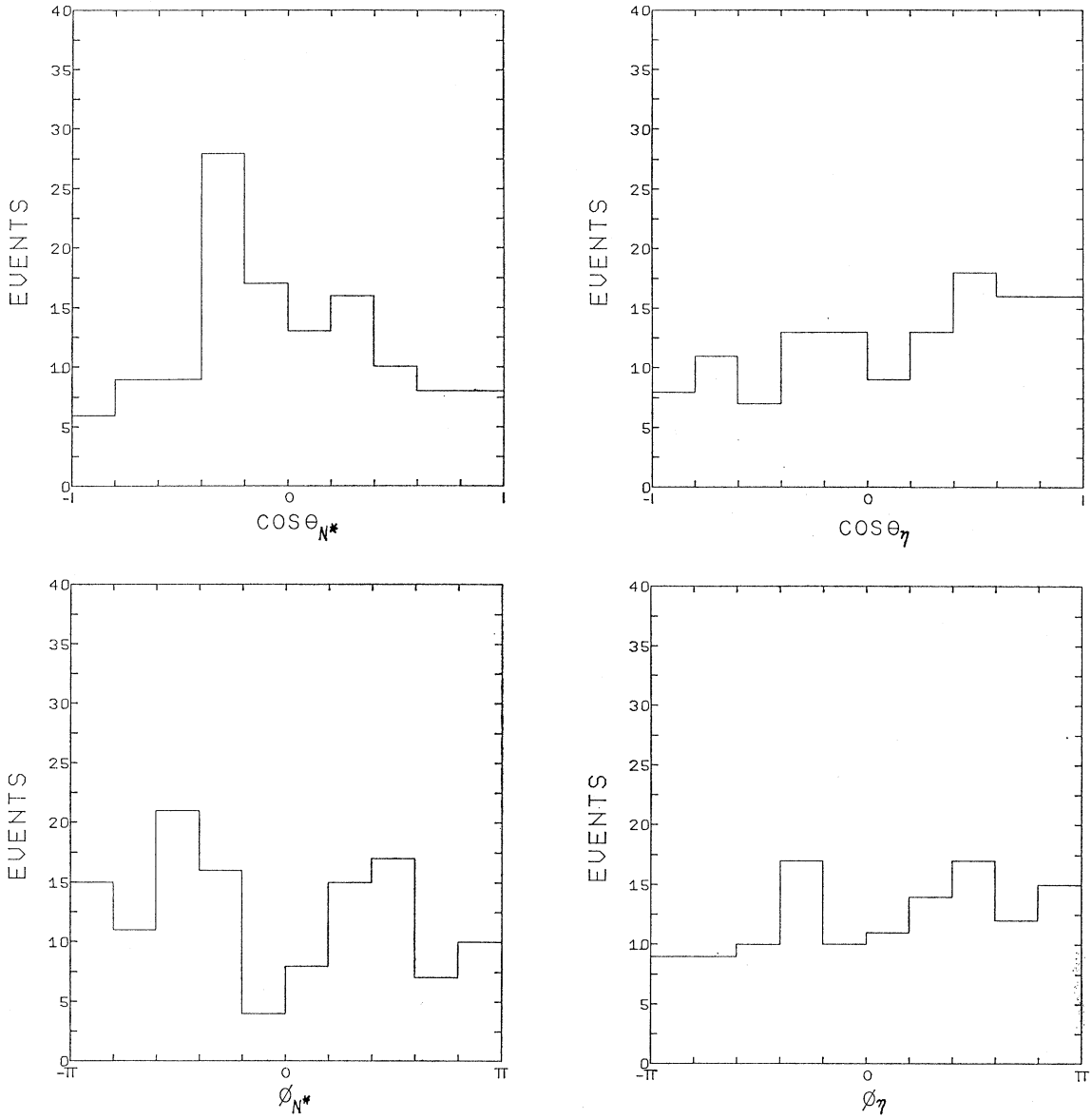

FIG. 31. N^* (left) and η (right) decay angular distributions in the helicity frame.

ACKNOWLEDGMENTS

We wish to thank the scanning and measuring staff for their diligent efforts under the direction of P. Wesley Weber and Mrs. Mary Null, the data handling group under H. White, and the bubble chamber staff under G. Eckman. The assistance of Professor Robert P. Ely, Jr., and Dr. George Kalmus in early aspects of this experiment is acknowledged. Finally, we appreciate the valuable discussions with Professor J. D. Jackson.